


RESEARCH

Open Access



The role of PKM2-mediated metabolic reprogramming in the osteogenic differentiation of BMSCs under diabetic periodontitis conditions

Yanlin Zhu^{1,2,3}, Yuhan Yang^{1,2,3}, Yuyan Lan^{1,2,3}, Zun Yang^{1,2,3}, Xiang Gao^{1,2,3} and Jie Zhou^{1,2,3*} 

Abstract

Background Diabetes mellitus (DM) and periodontitis have a bidirectional relationship, with each being a high-risk factor for the other. Prolonged hyperglycemia exacerbates periodontal inflammation and disrupts bone homeostasis. Pyruvate kinase M2 (PKM2), a key enzyme in glycolysis, is involved in metabolic reprogramming, but its role in osteogenesis under high-glucose (HG) inflammatory conditions remains largely unknown. This study aimed to investigate the effects of HG and inflammation on bone marrow mesenchymal stem cells (BMSCs) under indirect co-culture conditions and to explore how PKM2 regulates metabolism and mitochondrial function during osteogenic differentiation in HG inflammatory environments, elucidating its role in diabetic periodontitis (DP).

Methods Expose BMSCs to conditioned medium (CM) collected from RAW264.7 cells stimulated with HG and/or lipopolysaccharide (LPS). BMSCs functionality was assessed using CCK8, EdU, Annexin V-PI apoptosis assay, alkaline phosphatase (ALP), and Alizarin Red S (ARS) staining. Metabolic characteristics were evaluated through Seahorse assays, lactate production, glucose uptake, and ATP measurements. Mitochondrial function was assessed via JC-1, and ROS staining, Mito-Tracker staining, and transmission electron microscopy (TEM). Gene and protein expression were analyzed by quantitative real-time PCR and western blotting. In vivo therapeutic effects of shikonin were validated via micro-CT and histological staining in a diabetic periodontitis mouse model.

Results In vitro experiments demonstrated that HG inflammatory conditions impaired the survival of BMSCs, suppressed osteogenic differentiation, and induced metabolic reprogramming. This reprogramming was characterized by enhanced glycolysis, impaired oxidative phosphorylation (OXPHOS), abnormal upregulation of PKM2 expression, and mitochondrial dysfunction accompanied by morphological alterations. Shikonin effectively reversed these adverse effects by inhibiting PKM2 tetramerization, rescuing the loss of osteogenic function in BMSCs. The therapeutic potential of shikonin was confirmed in the diabetic periodontitis mouse model.

Conclusion PKM2 impairs the osteogenesis of BMSCs by affecting metabolism and mitochondrial function, suggesting it as a potential therapeutic target for diabetic periodontitis.

*Correspondence:

Jie Zhou
zhoujie_ortho@hospital.cqmu.edu.cn

Full list of author information is available at the end of the article



© The Author(s) 2025. **Open Access** This article is licensed under a Creative Commons Attribution-NonCommercial-NoDerivatives 4.0 International License, which permits any non-commercial use, sharing, distribution and reproduction in any medium or format, as long as you give appropriate credit to the original author(s) and the source, provide a link to the Creative Commons licence, and indicate if you modified the licensed material. You do not have permission under this licence to share adapted material derived from this article or parts of it. The images or other third party material in this article are included in the article's Creative Commons licence, unless indicated otherwise in a credit line to the material. If material is not included in the article's Creative Commons licence and your intended use is not permitted by statutory regulation or exceeds the permitted use, you will need to obtain permission directly from the copyright holder. To view a copy of this licence, visit <http://creativecommons.org/licenses/by-nc-nd/4.0/>.

Keywords Diabetes periodontitis, PKM2, Osteogenic differentiation, Metabolic reprogramming, Mitochondrial dynamics

Introduction

Diabetes mellitus (DM) is a metabolic disease characterized by chronic hyperglycemia, caused by an absolute or relative deficiency in insulin secretion, predominantly manifesting as type 2 diabetes. Prolonged metabolic disturbances lead to various complications, among which periodontitis is recognized as the sixth complication of diabetes and has garnered significant attention [1]. Periodontitis is a chronic oral inflammatory disease driven by the host's inadequate immune response to bacteria-induced inflammation, gradually damaging periodontal tissues and ultimately resulting in tooth loosening and loss. Previous mechanistic studies have demonstrated that the diabetic environment provokes an excessive inflammatory response to periodontal microbiota, accelerating periodontal destruction and impairing periodontal repair [2]. Diabetic periodontitis (DP) often presents severe inflammation and resistance to conventional periodontal treatments, creating considerable challenges in clinical management [3]. Currently, clinical outcomes for diabetic periodontitis patients are still limited, and it remains difficult to restore periodontal bone homeostasis.

Periodontal bone homeostasis is maintained through a delicate balance between osteoclast-mediated bone resorption and osteoblast-mediated bone formation. As precursors to osteoblasts, mesenchymal stem cells (MSCs) are crucial for maintaining bone homeostasis. When the osteogenic differentiation function of MSCs is impaired, this balance is disrupted, leading to reduced bone formation and bone loss. As MSCs require significant energy to sustain bone homeostasis [4], energy metabolism serves as a critical regulatory factor in their differentiation [5–7]. Distinct metabolic patterns are observed across various cell differentiation lineages and their associated functions [8]. Metabolic reprogramming is an adaptive regulation of cellular energy demands in response to varying environmental conditions to achieve new functions, which is commonly found in tumor cells and macrophages [9, 10]. However, in the context of diabetic periodontitis, which is characterized by elevated blood glucose levels and a chronic inflammatory environment, the metabolic properties of MSCs remain insufficiently explored.

Pyruvate kinase (PK) is the final and rate-limiting enzyme of glycolysis, and PKM2 is one of its four isoforms (PKM1, PKM2, PKL, and PKR), primarily expressed in proliferating cells in the form of inactive monomers, low-activity dimers, and active tetramers [11]. Some studies have shown that PKM2 can be highly

expressed in inflammatory responses, and pharmacological or genetic inhibition of its activity can prevent the initiation of inflammatory cascades [12–14]. In addition to its classical glycolytic role, PKM2 possesses unique non-glycolytic functions, exhibiting protein kinase activity. Growing evidence suggests that mitochondrial dysfunction is a key factor in the progression of various diseases [15–17]. As a protein kinase, PKM2 may regulate mitochondrial physiological processes, positioning it as a potential therapeutic target for cancer, inflammation, and related conditions [18, 19].

This study aimed to explore the impact of a high-glucose (HG) inflammatory microenvironment on BMSCs function by simulating such conditions, focusing on the role and mechanism of PKM2 in BMSCs osteogenic differentiation. This research could provide new insights into the molecular mechanisms underlying the progression of diabetes-associated periodontitis, as well as offer novel perspectives for the treatment of diabetic periodontitis patients.

Materials and methods

Cell culture and identification

As previously described [20], primary mouse BMSCs were isolated and collected in α -MEM (C12571500BT, Gibco, USA) supplemented with 10% FBS (BBP5, Moregate, New Zealand) and 1% penicillin-streptomycin solution (C0222, Beyotime, China). The cells were cultured at 37 °C with 5% CO₂. When the cells reached 80% confluence, they were passaged. After passage to the third generation, the BMSCs were seeded into plates at different ratios according to experimental needs. The surface markers of BMSCs (including CD34, CD45, CD73, CD90, and CD105) were detected by flow cytometry. The morphology of the BMSCs was observed under a fluorescence microscope after staining with phalloidin (40735ES, Yeasen, China). To evaluate their differentiation potential, BMSCs were cultured in osteogenic or adipogenic induction medium for 14 days.

Cell treatment

To establish an in vitro model of HG and/or inflammation, RAW264.7 cells were exposed to complete medium containing HG (35 mmol/L) and/or LPS (1 μ g/mL) (SMB00610, Sigma, USA) for 12 h. After stimulation, the supernatant was discarded, and the cells were washed with PBS. The cells were then cultured in normal complete medium for an additional 12 h. The supernatants from each group were collected, centrifuged at 1200 rpm for 5 min, and mixed with either normal complete

medium or osteogenic differentiation medium at specific ratios to prepare macrophage-conditioned medium (CM). Shikonin (HY-N0822, MCE, USA) and dorsomorphin (HY-13418 A, MCE, USA) were dissolved in DMSO and then diluted with culture medium to final working concentrations of 0.5 μ M and 5 μ M, respectively. Additionally, metformin (HY-B0627, MCE, USA) powder was dissolved in PBS to prepare a stock solution, with a working concentration maintained at 0.2 μ M during use.

Cell viability

The viability of BMSCs was assessed using the CCK-8 assay. BMSCs were seeded into 96-well plates at a density of 5×10^3 cells per well and incubated overnight, after which the medium was changed to conditioned medium. After incubation for 1, 3, or 5 days, 10 μ L of CCK-8 solution (C0038, Beyotime, China) was added to each well and incubated for 2 h. The optical density was measured at 450 nm using a multifunctional microplate reader.

EdU staining

DNA replication activity was evaluated using the EdU cell proliferation detection kit (C0075S, Beyotime, China) to further confirm the proliferation rate of BMSCs. After 3 days of treatment, BMSCs were labeled, fixed, washed, permeabilized, and stained according to the manufacturer's instructions, and images were captured under a fluorescence microscope.

Cell apoptosis

Cell apoptosis was analyzed by flow cytometry using an Annexin V-FITC and PI detection kit (C1062M, Beyotime, China). BMSCs were digested, collected, and incubated in the dark for 20 min with a mixture containing

Annexin V-FITC and PI, followed by detection using a flow cytometer. The total apoptosis rate was calculated as the sum of the apoptosis rates observed in the lower right quadrant (early apoptotic cells) and the upper right quadrant (late apoptotic/necrotic cells).

ALP, ARS staining, and semiquantitative analysis

The BMSCs were subjected to osteogenic induction for 7 or 14 days. After induction, the cells were washed with PBS (PB2004Y, TBD, China), and then fixed with 4% paraformaldehyde for 15 min, followed by additional PBS washes. A BCIP/NBT alkaline phosphatase color development kit (C3206, Beyotime, China) and an ARS staining kit for osteoblast mineralized nodules (C0148S, Beyotime, China) were used to stain the cells according to the manufacturers' protocols. The stained cells were observed and imaged under a standard microscope. Semiquantitative analysis of ALP staining was performed using ImageJ software, and after dissolving the deposited calcium salts in 10% cetylpyridinium chloride (CPC, C129534, Aladdin, China), the absorbance was measured at 562 nm for semiquantitative analysis of the ARS staining results.

Real-time quantitative PCR

Total RNA was extracted from the cells using TRIzol reagent (15596018, Invitrogen, USA). RNA concentration and purity were measured using a NanoDrop One Micro UV-Vis spectrophotometer (Thermo Fisher Scientific, USA). According to the manufacturer's instructions, cDNA was synthesized using the GoScript™ Reverse Transcription System (A5001, Promega, USA). qPCR was performed using cDNA mixed with SYBR green (A6001, Promega, USA) and primers at a final concentration of 10 μ M. Gene expression levels were normalized to the endogenous expression level of β -actin, and the data were analyzed using the $2^{-\Delta\Delta C_t}$ method. The primer sequences are listed in Table 1.

Western blotting

Total protein was obtained by lysing cells with RIPA lysis buffer (P0013B, Beyotime, China) mixed with PMSF (ST506, Beyotime, China), with additional sonication to facilitate cell lysis. The protein concentration was measured using a BCA protein assay kit (P0012, Beyotime, China). Equal amounts of protein were electrophoresed on 7.5% /10% /12.5%SDS-PAGE gels (PG111/PG112/PG113, EpiZyme, China) and transferred to PVDF membranes (FFP28, Beyotime, China). The membranes were blocked with 5% BCA at room temperature for 2 h. The membranes were incubated with antibodies specific for ALP (1:1000, ABclonal, China), RUNX2(1:1000, Abcam, UK), LDHA(1:1000, CST, USA), PFKFB3(1:1000, CST, USA), PKM2(1:1000, CST, USA), MFN2(1:1000, CST,

Table 1 Primer sequences used for qRT-PCR

Gene	primer F/R	sequence 5'–3'
RUNX2	F	GGGAACCAAGAAGGCACAGA
RUNX2	R	GGATGAGGAATGCGCCCTAA
ALP	F	ATCGACGTGATCATGGGTGG
ALP	R	TGGGAATGCTTGTGTCTGGG
LDHA	F	GCTACACGTACACGGAGACCT
LDHA	R	GAGGGTTGCCATCTTGAGCT
PFKFB3	F	CGGGTACAGAAGATCTGGGTG
PFKFB3	R	TACTGCTTCACAGCCTCACG
PKM2	F	ACGAGAACATCCTGTGGCTG
PKM2	R	GAAGTCAGCGCCTTCTCTCT
MFN2	F	TTCTTGTGGTCCGAGGAGTG
MFN2	R	CTTTGGTGGTCCAGGTGAGT
OPA1	F	CCGAGGATAGCTTGAGGGTT
OPA1	R	CGTTCTTGGTTTCGTTGTGA
DRP1	F	GGACATCATCCAGCTGCCTC
DRP1	R	TAGGCTTTCCAGCACTGAGC
FIS1	F	AGCTGGAACGCCTGATTGAT
FIS1	R	TGGAGACAGCCAGTCCAATG
β -actin	F	CAGCCTTCTTCTTGGGTAT
β -actin	R	TGGCATAGAGGTCTTTACGG

USA), OPA1(1:1000, Abcam, UK), DRP1(1:1000, CST, USA), FIS1(1:1000, CST, USA), AMPK(1:500, ZenBio, China), and p-AMPK (1:500, ZenBio, China), overnight at 4 °C. After three PBST washes, the membranes were incubated with secondary antibodies at 37 °C for 2 h. ECL solution (P0018AM, Beyotime, China) was prepared, and the bands were scanned and imaged in a dark room. ImageJ software was used to quantify the results. β -actin(1:1000, CST, USA) was used as the internal control.

Seahorse metabolic profile assay

The cells were digested and seeded into XFp probe plates at a density of 3×10^4 cells per well for adherence. The medium was replaced with XF base medium supplemented with 2 mM glutamine and 1 mM pyruvate, with or without 10 mM glucose, followed by incubation in a CO₂-free incubator for 1 h. For the XF Mito Stress Test, oligomycin, trifluoromethoxy carbonylcyanide phenylhydrazide (FCCP), antimycin A, and rotenone (103010-100, Agilent, USA) were prepared in XF base medium, with final concentrations of 1.5 mM oligomycin, 1.0 μ M FCCP, and 0.5 μ M antimycin A and rotenone. For the XF glycolytic stress test, glucose (10 mM), oligomycin (1.0 μ M), and 2-deoxy-D-glucose (2DG, 50 mM) (103017-100, Agilent, USA) were prepared and added to the plate for testing. Oxygen consumption rate (OCR) and extracellular acidification rate (ECAR) were normalized to the cell count. Related parameters were calculated and analyzed according to the manufacturer's instructions.

Lactate measurement

The original medium was removed, and the cells were washed with PBS before adding serum-free medium. The cells were incubated for 90 min, and the supernatant was collected. Lactate levels were measured via an L-lactate (L-LD) assay kit (A019-2-1, Nanjing Jiancheng Bioengineering Institute, China) following the manufacturer's protocol.

Glucose uptake

The BMSCs were digested, collected, and incubated in the dark at 37 °C with 2-Deoxy-2-[(7-nitro-2,1,3-benzoxadiazol-4-yl)amino]-D-glucose (2-NBDG, 11046, Cayman, USA) at a working concentration of 200 μ M for 30 min. The uptake of glucose was analyzed using flow cytometry.

ATP measurement

The original medium was removed, and the cells were washed with PBS. An appropriate amount of lysis buffer (S0026, Beyotime, China) was added, and the supernatant was collected after cell lysis. A 100 μ L ATP detection reagent was added to the wells, followed by a 5-minute

incubation at room temperature. Then, 20 μ L of the supernatant from the test samples was added to each well and mixed thoroughly. The relative light units (RLU) were measured using a luminometer.

DSS crosslinking

The samples were crosslinked with 5 mM disuccinimidyl suberate (DSS, 21555, Thermo Scientific, USA) at room temperature for 30 min. Afterward, 1 M Tris-HCl (pH=7.5) was added to a final concentration of 20 mM, and the reaction was quenched by incubation at room temperature for 15 min. The lysates were analyzed by western blotting.

Immunofluorescence staining

After treatment, the samples were fixed in 4% paraformaldehyde for 15 min, permeabilized with 0.2% Triton X-100 for 20 min, and blocked with 2% BSA for 30 min. The samples were then incubated with anti-PKM2 (1:100, CST, USA), followed by incubation with the appropriate secondary antibody and DAPI. Immunofluorescence images were captured using laser scanning confocal microscopy (LSCM). The 3D surface plot was analyzed using ImageJ, where higher peaks indicated stronger staining intensity.

JC-1 and ROS staining

Mitochondrial function was measured using the JC-1 assay kit (C2003S, Beyotime, China) and ROS detection kit (D6883, Sigma, USA). The images were captured using a standard microscope or the fluorescence intensity was measured using flow cytometry.

Mito-Tracker staining

The BMSCs were incubated with 200 nM Mito-Tracker Red FM (C1032, Beyotime, China) at 37 °C for 30 min. After washing, the cells were cultured in medium, and mitochondrial morphology was examined via confocal microscopy. Mitochondrial length was analyzed using ImageJ.

Mitochondrial transmission electron microscopy

The cells were collected, centrifuged, and the supernatant was discarded. The cell pellet was fixed with pre-cooled 4% glutaraldehyde solution at 4 °C for temporary storage. The samples were subsequently fixed with 1% osmium tetroxide solution, dehydrated with a graded ethanol series, embedded, sectioned, stained, air-dried, and observed under a transmission electron microscope.

Mouse model of type 2 diabetes (T2DM)

Animal experiments were conducted following the ARRIVE (Animal Research: Reporting of In Vivo Experiments) guidelines and were approved by the Animal

Ethics Committee of Chongqing Medical University (Project: The Role of PKM2-Mediated Metabolic Reprogramming in the Osteogenic Differentiation of BMSCs under Diabetic Periodontitis Conditions, No. 2024-115, Date: 2024.07.19). Four-week-old male C57BL/6 mice were purchased from SJA Laboratory Animal CO.LTD (Hunan, China). The mice were housed in pathogen-free conditions and allowed to acclimate for one week before being fed a high-fat/high-glucose diet (HFHG, D12492, Research Diets, USA). After 8 weeks of feeding, the mice reached a body weight of 32–38 g and were intraperitoneally injected with streptozotocin (STZ, 40 mg/kg, S0130, Sigma, USA) for 5 consecutive days. One week after the last injection, relevant parameters were measured. Mice with fasting blood glucose levels above 16.7 mM and clinical symptoms (increased food and water consumption, increased urine output, and weight loss) were diagnosed with T2DM. The work has been reported in line with the ARRIVE guidelines 2.0.

Experimental periodontitis model

After the mice were anesthetized by intraperitoneal injection of 1% (w/v) pentobarbital sodium solution (50 mg/kg, Notlas, China), a 5–0 silk ligature was inserted between the maxillary first and second molars, with both ends tied in a knot, and left in place for 14 days. The ligature was checked every two days for loosening or dislodgment, and if dislodged, a new ligature was inserted promptly.

Animal group allocation

The main result in subsequent studies is the distance between the distance of cemento-enamel junction (CEJ)-alveolar bone crest (ABC). According to published studies [21], the significant intergroup differences between the control group and the periodontitis group were 0.25 mm (standard deviation [SD]=0.05 mm) and 0.45 mm (SD=0.2 mm), respectively. With an 80% power, α of 0.05 and 2-tailed test, a sample size of 6 mice per group was recommended. Considering potential losses during the experimental process, we have ensured that each group contains 9 mice to maintain statistical power.

T2DM mice with successful modeling were randomly divided into three groups ($n=9$ per group):

- (1) Diabetes-only group;
- (2) Diabetes with periodontitis (DP) group (ligature-induced experimental periodontitis for 14 days);
- (3) DP + shikonin group (shikonin treatment for experimental diabetes with periodontitis for 14 days, with a frequency of once per day in the morning).

In another cohort, normal male C57BL/6 mice of the same age as the T2DM group were divided into three groups ($n=9$ per group):

- (1) Control group (no treatment);

- (2) Control + shikonin group (treated with shikonin for 14 days, with a frequency of once per day in the morning and evening);

- (3) Experimental periodontitis (EP) group (ligature-induced experimental periodontitis for 14 days).

The total effective animal sample size for this experiment was 54.

In vivo drug administration

Polyether F127 diacrylate (F127DA, EFL-F127DA-001, EngineeringForLife, China), a commonly used hydrogel with thermogelation properties that can be used to carry hydrophobic drugs, was chosen as the delivery vehicle for shikonin. A suitable amount of F127DA was dissolved in a shikonin solution at a final concentration of 0.5 mg/mL (ensuring that the final concentration of F127DA was 20%), thoroughly stirred in an ice bath, and then mixed with an appropriate initiator. The mixture was filtered under cold conditions and injected it into the periodontal area between the maxillary first and second molars using a microsyringe after anesthesia in mice. The gel was cured using 405 nm blue light for approximately 30 s. Mice in the diabetes-only, DP and EP groups were injected with an equal amount of PBS at the same site, while the control group received no treatment.

Fasting blood glucose and OGTT test

After overnight fasting (water allowed), the mouse tail tip was cut by 1 mm with scissors, and a small amount of tail blood was collected to measure fasting blood glucose levels using a glucometer and glucose test strips. A sucrose solution (200 mg/mL) was prepared and administered via gavage (2 g/kg). Blood glucose levels were recorded at 30, 60, 90, and 120 min.

Micro-CT

Euthanized mice using CO₂. In short, placed the mice in a cage and ensured that the CO₂ gas flow rate replaces at least 20% of the cage volume per minute. Maintained this level for at least three minutes until the mice were confirmed dead. The maxillae were separated and scanned using micro-CT (vivaCT80, SCANCO Medical AG, Switzerland). The scanning parameters were set at 70 kV and 112 μ A, with a slice thickness of 10 μ m. The proximal region between the maxillary first and second molars was selected as the region of interest (ROI). Using SCANCO VivaCT40 micro-CT software, the distance from the cemento-enamel junction to the alveolar bone crest (CEJ-ABC), the percentage of bone volume per unit tissue volume (BV/TV), the number of trabeculae (Tb.N), and trabecular thickness (Tb.Th) were analyzed.

Histological analysis

All samples were fixed in 4% paraformaldehyde solution for 36 h and decalcified in 10% ethylene diamine tetraacetic acid (EDTA) for 5 weeks. The maxillary bone specimens were then embedded in paraffin, and 6 μ m-thick sections were prepared. Hematoxylin and eosin (H&E) staining was used to assess periodontal conditions, Masson's trichrome staining was used to evaluate the degree of periodontal inflammation, and tartrate-resistant acid phosphatase (TRAP) staining was used to examine osteoclast activity. The expression of target proteins was observed using immunohistochemistry and immunofluorescence staining.

Statistical analysis

All experiments were repeated at least three times, and the results were expressed as mean \pm SEM. An unpaired t-test was used to analyze two independent groups. For multiple comparisons, one-way analysis of variance (ANOVA) followed by Tukey's post hoc test was performed. Statistical analysis was conducted using GraphPad Prism software (version 8.0.2, USA). A P-value of less than 0.05 (* P < 0.05, ** P < 0.01, *** P < 0.001, and **** P < 0.0001) was considered statistically significant.

Results

The presence of CM-HG exacerbates BMSCs damage caused by the inflammatory microenvironment

Flow cytometry analysis identified undifferentiated BMSCs as positive for CD73, CD90, and CD105 (mesenchymal stem cell markers) and negative for CD34 and CD45 (hematopoietic cell markers) (Fig. S1A). Under a microscope, undifferentiated BMSCs appeared spindle-shaped or polygonal, and staining with phalloidin revealed that BMSCs attached and spread on culture plates (Fig. S1B). After being cultured in their respective induction media, isolated BMSCs demonstrated osteogenic and adipogenic potential (Fig. S1C, D).

To better simulate the diabetic periodontal immune microenvironment, we used an indirect co-culture method, treating RAW264.7 cells with HG (35 mM) or/and LPS (1 μ g/ml) for 12 h, and then replaced with ordinary medium for further 12 h. The supernatant was collected to produce CM for subsequent BMSCs culture (Fig. 1A). We investigated whether HG levels amplify the effects of inflammatory microenvironment on BMSCs activity and function.

According to CCK-8 assay results, there was no significant change in BMSCs activity on days 1 and 3 after treatment with macrophage-conditioned medium prepared under high-glucose conditions (CM-HG), but by day 5, activity was relatively reduced. BMSCs activity exhibited a consistent downward trend following treatment with macrophage-conditioned medium prepared under LPS

conditions (CM-LPS) throughout the observation period. Moreover, we observed that the macrophage-conditioned medium prepared under high-glucose and LPS conditions (CM-HG + LPS) markedly reduced the viability of BMSCs upon exposure (Fig. 1B). After three days of stimulation, we conducted EdU assays, which confirmed the CCK-8 results (Fig. 1C). To further confirm the effects of the HG inflammatory environment on BMSCs apoptosis, we used Annexin V-PI staining and flow cytometry. The results indicated that CM-LPS treatment greatly increased BMSCs apoptosis, and this phenomenon was more pronounced in BMSCs treated with CM-HG + LPS (Fig. 1D). To evaluate the damage of CM-HG + LPS treatment on the osteogenic differentiation ability of BMSCs, we respectively performed ALP and ARS staining on days 7 and 14 after osteogenic induction. Both ALP and ARS staining yielded similar results, indicating that the HG inflammatory microenvironment drastically reduced the osteogenic differentiation potential of BMSCs (Fig. 1E, F). Subsequent validation at the gene and protein levels confirmed this finding (Fig. 1G, H). These results suggest that CM-HG treatment adversely affects BMSCs activity and function, amplifying the damaging effects of CM-LPS treatment.

CM-HG + LPS treatment induces metabolic reprogramming in cells

According to studies, alterations in the extracellular environment can have an impact on cellular metabolism [22, 23]. Subsequently, we investigated the metabolic characteristics of BMSCs treated with CM-HG + LPS. Seahorse assays were employed to assess the metabolic state of BMSCs three days post-osteogenic induction. Results showed no significant changes in oxidative phosphorylation rates or related indicators among groups, while the glycolysis and glycolytic capacity in treatment groups significantly increased (Fig. 2A). Additionally, endpoint lactate measurements further confirmed the rise in glycolytic rates (Fig. 2B). Surprisingly, CM-HG or/and CM-LPS treatment boosted glucose absorption, and under these unfavorable stimuli, the total ATP production of BMSCs actually increased (Fig. 2C, D). We suspected that the short treatment duration might have contributed to unexpected results. Therefore, we repeated these assays 7 days post-osteogenic induction. Unlike previous results, we observed substantial variations in cellular oxygen consumption rate (OCR) between the CM-LPS treated group and the control group. After CM-HG + LPS treatment, it seems that this difference was amplified, reducing the basal OCR, FCCP-induced maximum OCR, and ATP-linked OCR. Differences in extracellular acidification rate (ECAR) among treatment groups also became more pronounced, with cells in CM-HG + LPS treatment groups exhibiting prominent glycolysis and glycolytic

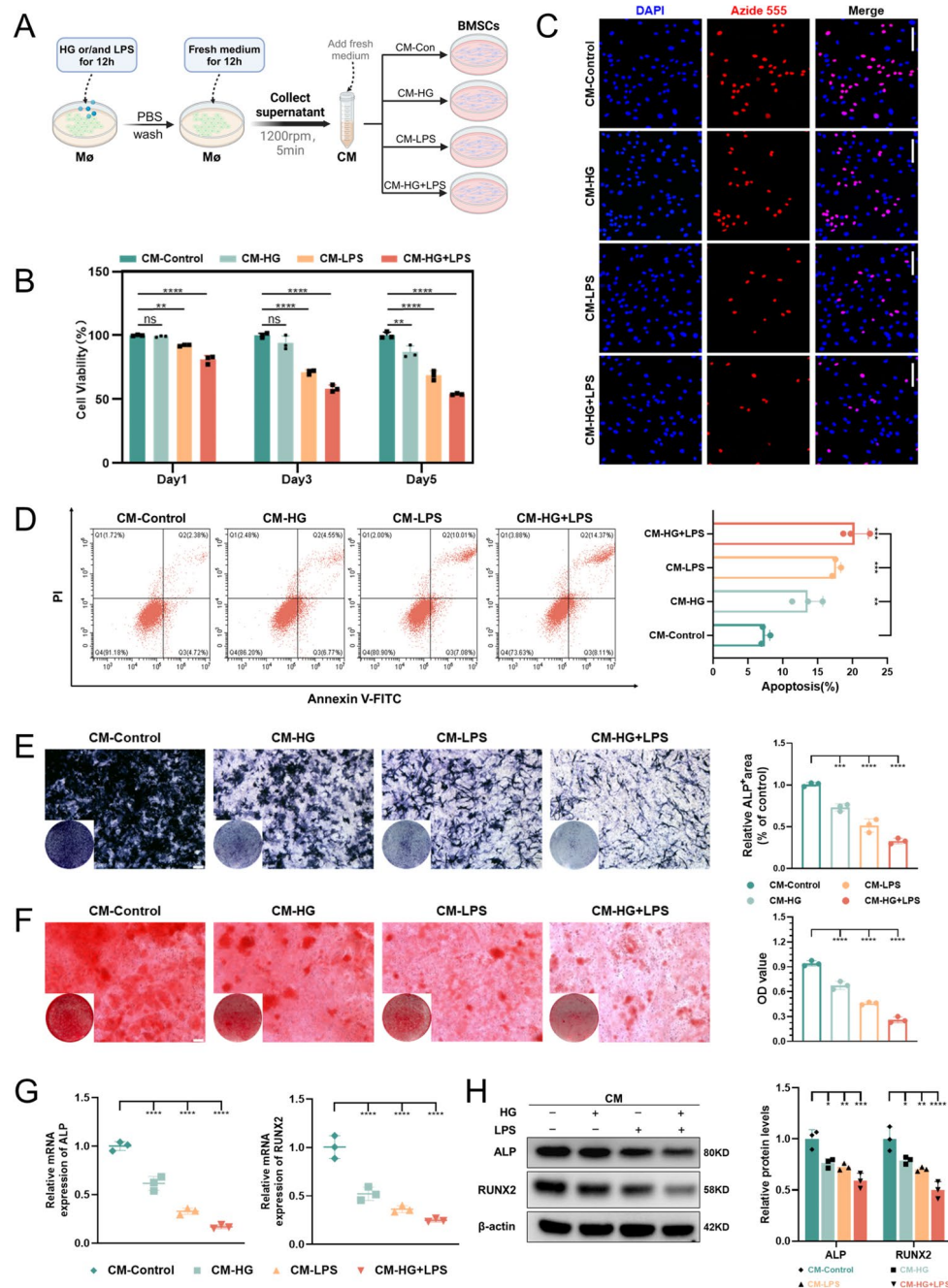


Fig. 1 The presence of CM-HG exacerbates BMSCs damage caused by the inflammatory microenvironment. **(A)** Experimental schematic for generating conditioned media for BMSCs culture (Images created with Biorender.com). **(B)** Cell viability assessed using the CCK-8 assay on days 1, 3, and 5. **(C)** EdU staining reflecting DNA replication activity of BMSCs after 3 days of culture (scale bar: 100 μm). **(D)** Flow cytometry analysis of apoptosis using Annexin V-FITC and PI staining. Apoptotic cells are represented as the percentage of Annexin V-positive and Annexin V/PI double-positive cells. **(E, F)** Osteogenic potential of BMSCs assessed by ALP staining on day 7 **(E)** and ARS staining on day 14 **(F)** (scale bar: 100 μm). Semiquantitative analysis of ALP staining was performed using ImageJ. Calcium deposition was evaluated by measuring optical density at 562 nm. **(G, H)** qPCR and western blot analysis of ALP and RUNX2 expression (β-actin was used as the internal control). Full-length blots are presented in Supplementary Fig. S3. * $P < 0.05$, ** $P < 0.01$, *** $P < 0.001$, **** $P < 0.0001$; ns, not significant

capacity, leading to a remarkable increase in acid production (Fig. 2E, F). Although all treatment groups maintained high glucose uptake compared to controls, total ATP production markedly decreased (Fig. 2G, H). This

indicates that BMSCs underwent metabolic reprogramming during osteogenic differentiation after CM-HG or/and CM-LPS treatment, shifting from reliance on OXPHOS to glycolysis while exhibiting high energy

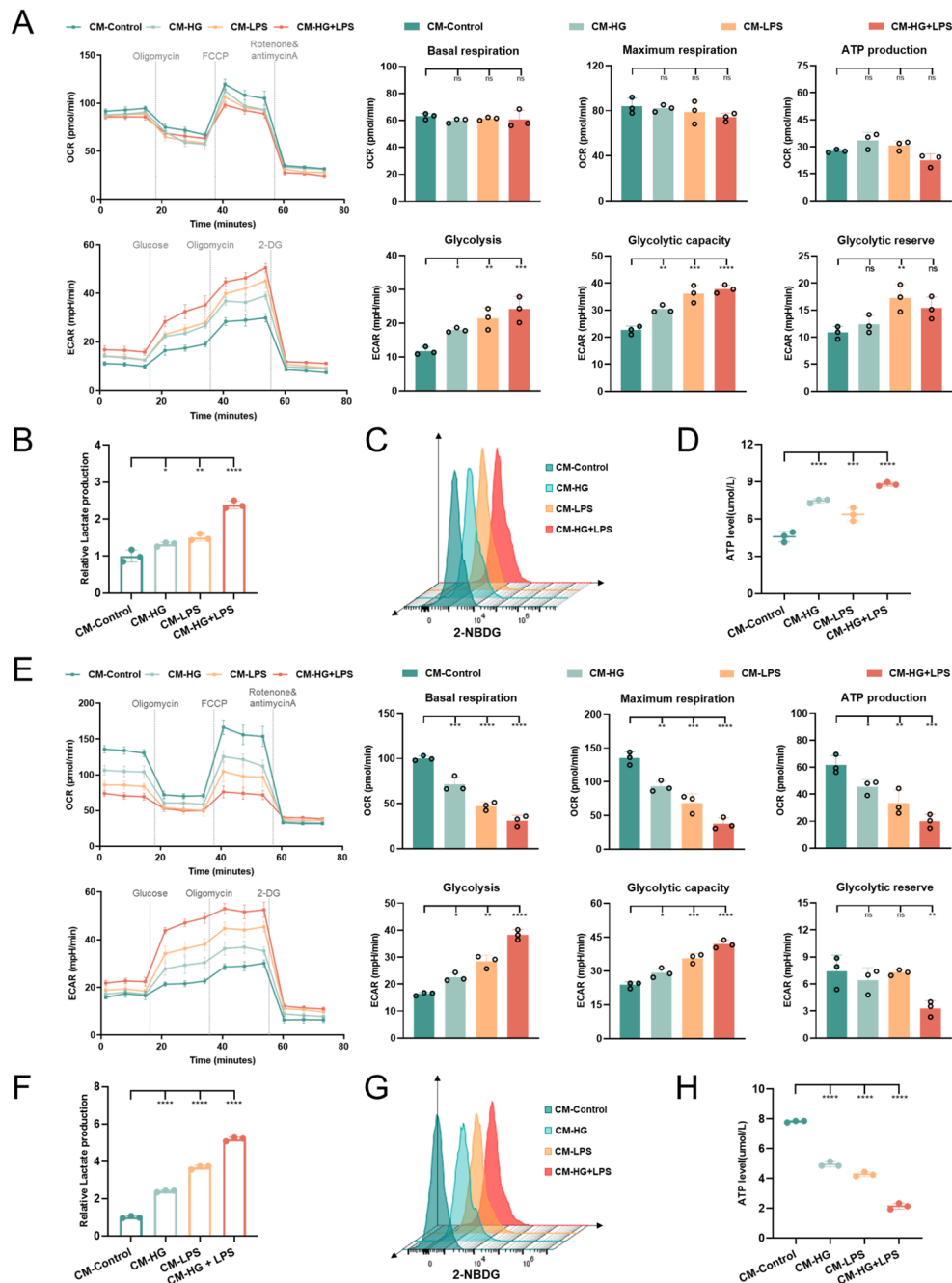


Fig. 2 CM-HG+LPS treatment induces metabolic reprogramming in cells. **(A)** Metabolic characteristics of BMSCs after 3 days of osteogenic induction. Basal respiration, maximum respiration, ATP production, basal glycolysis, glycolytic capacity, and glycolytic reserve are presented as bar graphs. **(B)** Relative lactate production in BMSCs on day 3 for each group. **(C)** On day 3, 2-NBDG was used as a fluorescent probe to compare glucose uptake between groups, with results presented as staggered offset histograms. **(D)** ATP concentration was assessed 3 days post-induction to compare total energy production between groups. **(E)** Metabolic characteristics of BMSCs after 7 days of osteogenic induction. Basal respiration, maximum respiration, ATP production, basal glycolysis, glycolytic capacity, and glycolytic reserve are presented as bar graphs. **(F)** Relative lactate production in BMSCs on day 7 for each group. **(G)** On day 7, 2-NBDG was used as a fluorescent probe to compare glucose uptake between groups, with results presented as staggered offset histograms. **(H)** Assessment of ATP concentration 7 days post-induction to compare the total energy production of each group. * $P < 0.05$, ** $P < 0.01$, *** $P < 0.001$, **** $P < 0.0001$, ns, no significance

consumption characteristics, albeit with impeded ATP synthesis.

The PKM2 tetramer likely mediates Glycolysis in cells under HG inflammatory microenvironment

We were intrigued by the phenomenon of increased glycolytic rates in BMSCs caused by CM-HG+LPS treatment. To validate this, we utilized quantitative real-time PCR and western blotting to detect levels of key enzymes involved in the glycolytic pathway within cells. Results

showed that CM-HG+LPS treatment upregulated the levels of LDHA, PFKFB3, and PKM2, which was consistent with previous assessments of glycolytic levels (Fig. 3A, B). Notably, in the CM-HG+LPS treated group, PKM2 expression significantly exceeded that of other groups. We hypothesize that the increased glycolysis induced by CM-HG+LPS treatment is primarily driven by PKM2. We then explored the specific conformation of PKM2. Through DSS crosslinking assays, we found that CM-HG+LPS treatment significantly induced the

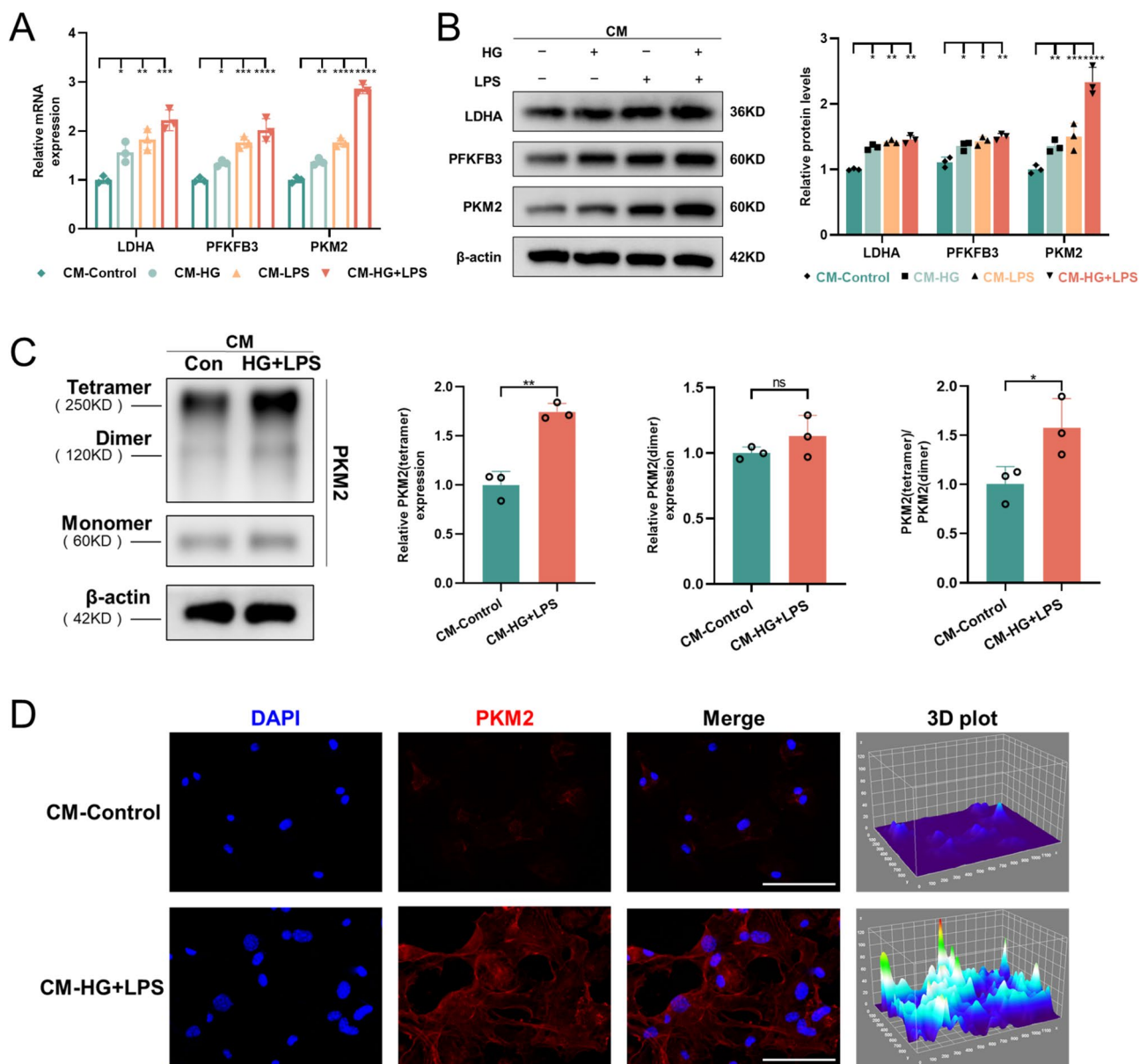


Fig. 3 The PKM2 tetramer likely mediates glycolysis in BMSCs under HG inflammatory microenvironment. **(A, B)** The relative expression of glycolysis-related genes and proteins (LDHA, PFKFB3, and PKM2) was assessed by qPCR and western blot analysis on day 7. Full-length blots are presented in Supplementary Fig. S3. **(C)** Quantification of relative protein expression levels of the PKM2 tetramer, PKM2 dimer, and the tetramer/dimer ratio in BMSCs, presented as bar graphs. Full-length blots are presented in Supplementary Fig. S3. **(D)** Representative fluorescence images and 3D surface plots showing PKM2 and nuclei in BMSCs (Nucleus: blue, PKM2: red; scale bar: 100 μ m). * P < 0.05, ** P < 0.01, *** P < 0.001, **** P < 0.0001; ns, not significant

expression of PKM2 tetramers, with no notable impact on PKM2 dimers or monomers (Fig. 3C). Immunofluorescence staining corroborated these findings. Under normal conditions, PKM2 is expressed at modest levels near the nucleus, but stimulation with CM-HG+LPS raised its expression in the cytoplasm raised its expression in the cytoplasm (Fig. 3D).

CM-HG + LPS treatment impairs mitochondrial function and alters mitochondrial morphology

We noticed that CM-HG+LPS treatment altered the metabolic characteristics of BMSCs during the osteogenic differentiation process. During this process, in addition to increased glycolysis, we also observed impaired mitochondrial OXPHOS pathways. We speculate that CM-HG+LPS treatment may exacerbate mitochondrial damage in the cells, thereby increasing the metabolic stress on the glycolytic pathway. Mitochondrial membrane potential and intracellular ROS levels are closely associated with mitochondrial function. First, we measured mitochondrial membrane potential (MMP) using the JC-1 probe and analyzed intracellular ROS levels via flow cytometry. The results showed that both CM-HG and CM-LPS treatments reduced MMP and increased ROS levels, with CM-HG+LPS treatment exhibiting the most significant disruption of mitochondrial function (Fig. 4A, B). Mito-Tracker staining revealed that the mitochondrial network structure was disrupted and fragmented under all treatments, with mitochondrial fragmentation being most pronounced in the CM-HG+LPS group (Fig. 4C). TEM showed that, compared to the other groups, mitochondria in cells treated with CM-HG+LPS exhibited pathological morphology, appearing smaller, swollen, or fragmented (Fig. 4D). Furthermore, we examined the expression of genes and proteins involved in mitochondrial dynamics. We observed that CM-HG+LPS treatment led to a decrease in MFN2 and OPA1, while enhancing the expression of FIS1 and DRP1 (Fig. 4E, F). In summary, CM-HG+LPS treatment impaired mitochondrial function and altered mitochondrial morphology.

Inhibition of PKM2 promotes mitochondrial fusion in BMSCs under HG inflammatory conditions, improving mitochondrial function

PKM2 has been reported to regulate energy metabolism and mitochondrial morphology [24]. We hypothesize that CM-HG+LPS treatment promotes the overexpression of PKM2, which mediates metabolic reprogramming while inducing changes in mitochondrial morphology and functional impairment. We investigated whether shikonin, as a PKM2 inhibitor, could ameliorate the impact of the HG inflammatory environment on mitochondrial function. We found that shikonin alone seemed to

promote mitochondrial elongation to some extent while rescuing the mitochondrial fragmentation induced by CM-HG+LPS (Fig. 5A). TEM also supported this finding, revealing that after treatment with shikonin, the mitochondrial morphology in cells appeared more regular and elongated (Fig. 5B). To further verify this result, we assessed changes in relevant genes and proteins using real-time quantitative PCR and western blotting. We observed that shikonin induced an increase in MFN2 and OPA1 levels while reducing the expression of DRP1 and FIS1 (Fig. 5C, D). Similarly, shikonin treatment alleviated changes in MMP in the CM-HG+LPS group, as seen by reduced green fluorescence and increased red fluorescence, and it decreased ROS production (Fig. 5E, F).

Shikonin mainly reverses cellular metabolic reprogramming by inhibiting PKM2 tetramer formation

To explore whether the protective effect of shikonin on BMSCs in the HG inflammatory environment is related to cellular metabolic reprogramming, we assessed the metabolic characteristics of cells treated with shikonin. Compared to previous experimental results, shikonin alleviated the inhibition of OCR brought on by CM-HG+LPS, modestly enhancing the basal respiration, maximum respiration, and ATP-linked of the cells. At the same time, it reduced the excessively high glycolysis and glycolytic capacity of the cells, while increasing glycolytic reserve to some extent (Fig. 6A). The release of lactate, the final product of glycolysis, was also inhibited (Fig. 6B). Shikonin reduced glucose uptake in stressed cells but increased the previously lowered total ATP levels (Fig. 6C, D). Compared to the CM-HG+LPS group, shikonin dramatically reduced the expression of LDHA, PFKFB3, and PKM2, further confirming its protective role against abnormal cellular metabolism, likely through the inhibition of PKM2's highly active state (Fig. 6E, F). DSS crosslinking experiments demonstrated that shikonin significantly inhibited the expression of PKM2 tetramers, with less effect on its dimeric and monomeric forms (Fig. 6G). Immunofluorescence analysis revealed comparable results, with shikonin suppressing the expression of PKM2, particularly in the cytoplasm (Fig. 6H).

Shikonin alleviates the inhibition of osteogenic function of BMSCs in HG inflammatory conditions by activating the AMPK pathway

Finally, we examined the effect of shikonin on the osteogenic function of cells in the HG inflammatory micro-environment. Shikonin has a valuable therapeutic effect on cells, as verified by ALP and ARS staining, quantitative PCR, and western blot experiments (Fig. 7A-D). Notably, shikonin also had a promoting effect on osteogenesis in BMSCs under normal circumstances.

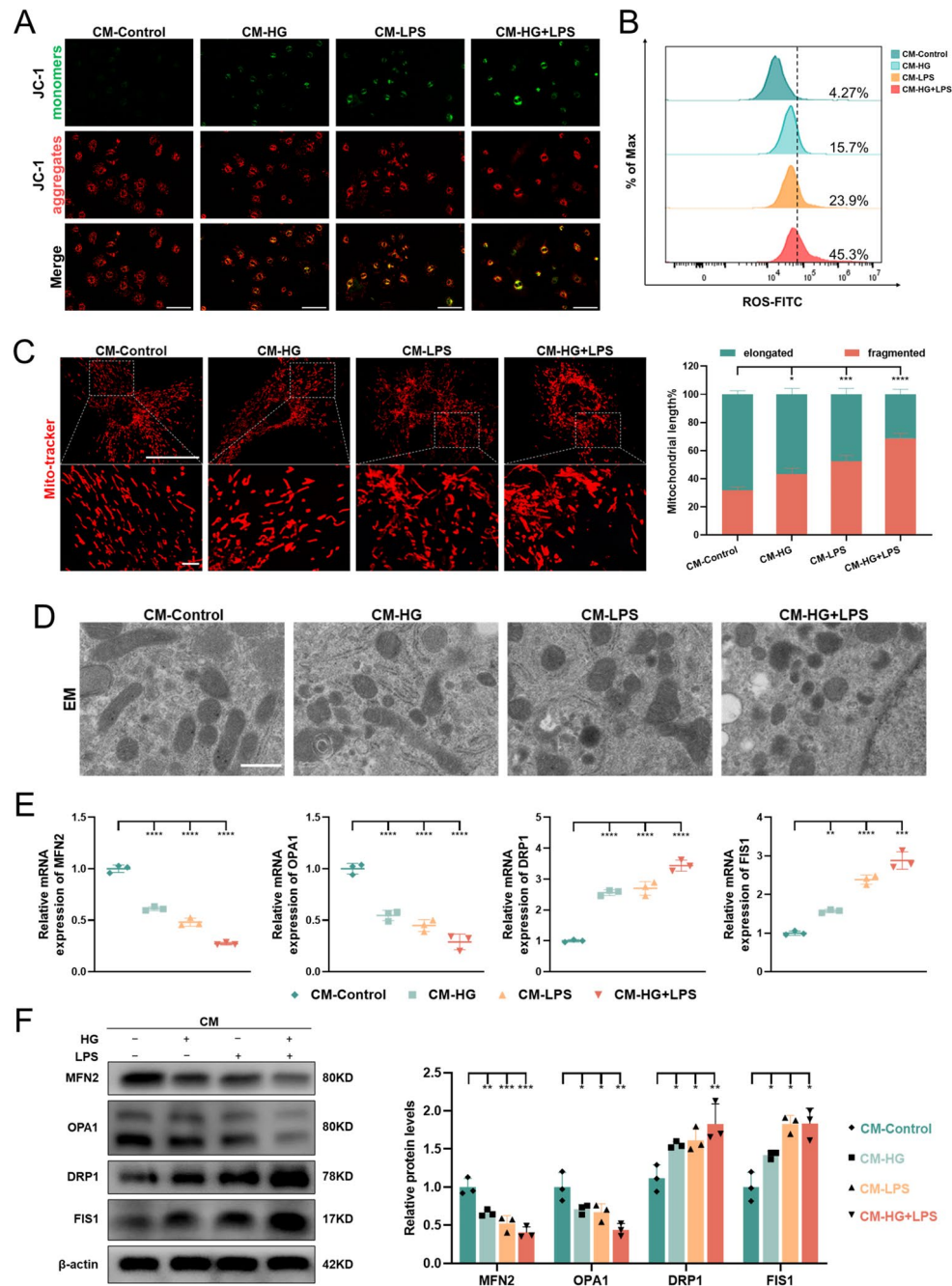


Fig. 4 CM-HG+LPS treatment impairs mitochondrial function and alters mitochondrial morphology. **(A)** Using JC-1 staining to assess mitochondrial membrane potential. Red and green fluorescence indicated JC-1 aggregates and monomers, respectively. (scale bar: 100 μ m). **(B)** Detection of intracellular ROS levels in BMSCs using the DCFH-DA probe and analyzed by flow cytometry. **(C, D)** Representative confocal and electron microscopy (EM) images indicated differences in mitochondrial morphology between groups. Mito-Tracker Red (red) was used in the confocal images to label cells that contain mitochondria. (scale bars for confocal imaging: 50 μ m. scale bars for EM: 500 nm). Images depicted representative fields from over ten cells photographed. Quantitative analysis of intracellular mitochondrial length using ImageJ. **(E)** qPCR analysis of mRNAs involved in mitochondrial fusion (MFN2 and OPA1) and mitochondrial fission (DRP1 and FIS1) in cultured BMSCs. **(F)** Expression of relevant protein levels was detected by western blotting. Full-length blots are presented in Supplementary Fig. S3. * $P < 0.05$, ** $P < 0.01$, *** $P < 0.001$, **** $P < 0.0001$; ns, not significant

AMP-activated protein kinase (AMPK) is a key regulator of cellular metabolism and energy balance, while also regulating mitochondrial dynamics [25] and closely associated with PKM2 [26]. When the AMPK pathway

is activated, it tends to promote osteogenesis [27, 28]. Therefore, we postulated that shikonin alleviates the suppression of osteogenic function in BMSCs under the HG inflammatory condition by activating the AMPK

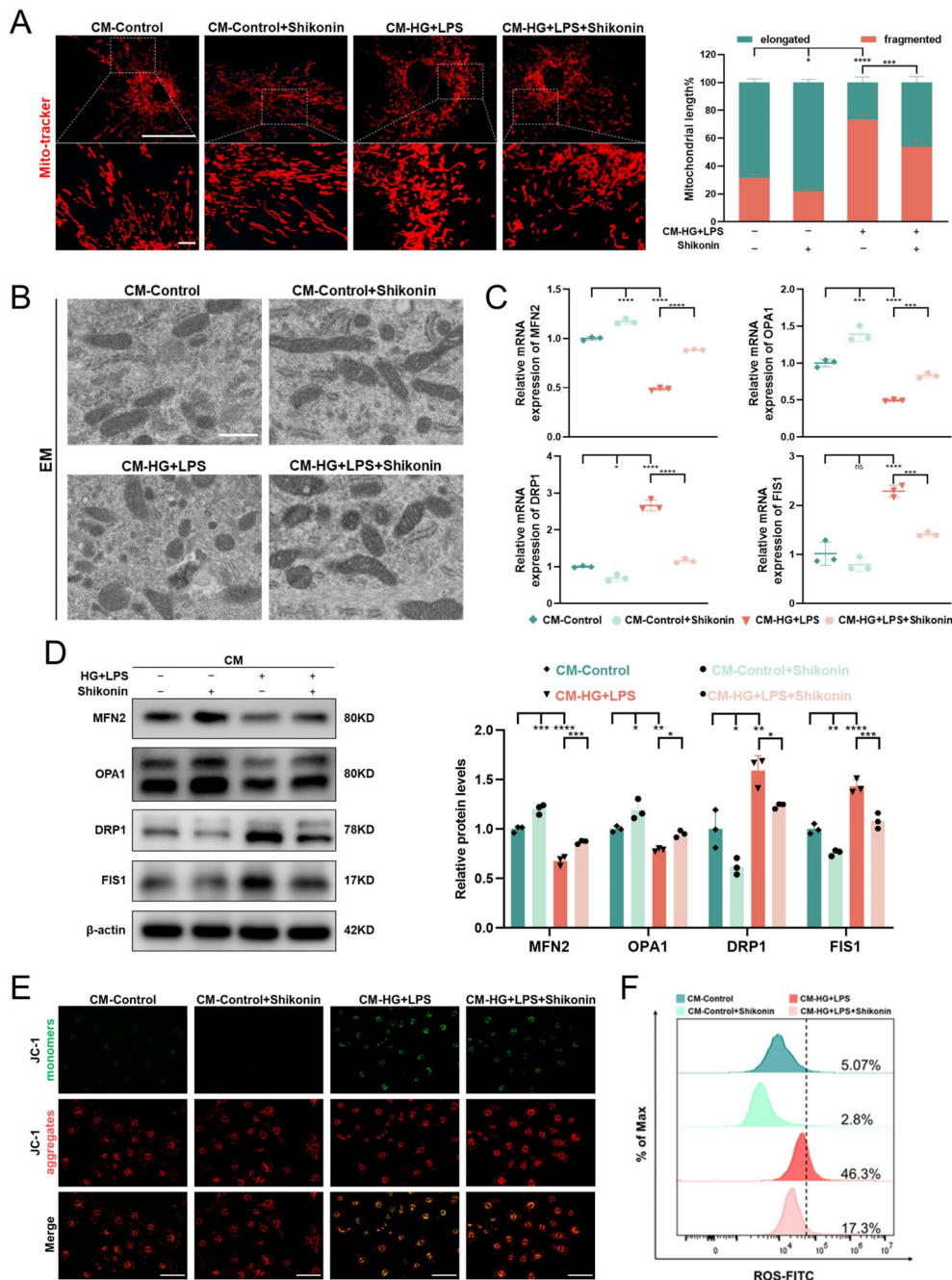


Fig. 5 Inhibition of PKM2 promotes mitochondrial fusion in BMSCs under HG inflammatory conditions, improving mitochondrial function. **(A, B)** Changes in mitochondrial morphology after the addition of shikonin, as demonstrated by representative confocal and EM images (scale bar for confocal images: 50 μ m; scale bar for EM: 500 nm). Quantitative analysis of mitochondrial length was performed based on confocal images, with 10 images analyzed per group. **(C)** Expression of mitochondrial fusion genes (MFN2 and OPA1) and fission genes (DRP1 and FIS1) after shikonin treatment. **(D)** Protein levels of mitochondrial fusion genes (MFN2 and OPA1) and fission genes (DRP1 and FIS1) after shikonin intervention, as assessed by western blotting. Full-length blots are presented in Supplementary Fig. S4. **(E)** Representative JC-1 staining image after shikonin treatment in BMSCs (scale bar: 100 μ m). **(F)** Flow cytometry analysis of intracellular ROS levels in BMSCs stained with DCFH-DA. * $P < 0.05$, ** $P < 0.01$, *** $P < 0.001$, **** $P < 0.0001$; ns, not significant

pathway. Subsequent Western blot investigations validated this viewpoint, showing that the intervention of CM-HG + LPS severely inhibited the activation of the AMPK pathway (Fig. 7E). Additionally, we conducted further validation using both an AMPK activator and

inhibitor. Results showed that adding the AMPK activator metformin rescued the osteogenic function of BMSCs, while the inhibitor dorsomorphin weakened the effect of shikonin on AMPK activation and reversed its promoting effect on the osteogenic differentiation

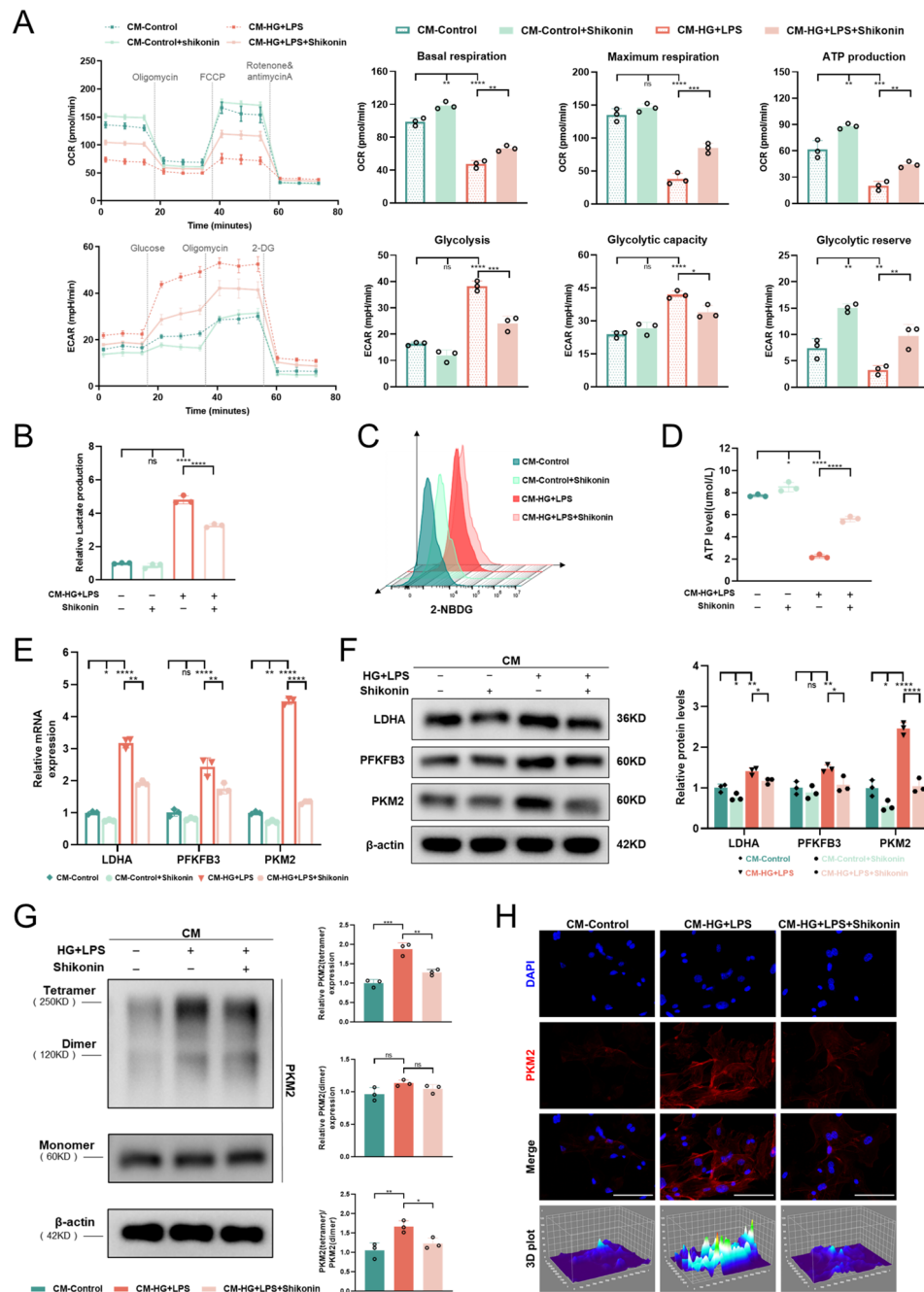


Fig. 6 Shikonin reverses cellular metabolic reprogramming primarily by inhibiting PKM2 tetramer formation. **(A)** Comparison of cellular metabolic characteristics with and without shikonin treatment. Basal respiration, maximum respiration, ATP production, basal glycolysis, glycolytic capacity, and glycolytic reserve are presented as bar graphs. (Dashed line groups represented data from Fig. 2E, specifically the values for the CM-Control group and CM-HG+LPS group). **(B)** Differences in relative lactate production rates in BMSCs before and after shikonin treatment. **(C)** Glucose uptake in BMSCs detected using the 2-NBDG probe, as shown in the histogram, with or without shikonin treatment. **(D)** ATP concentration used to assess the impact of shikonin on total cellular energy production. **(E)** The effect of shikonin on the gene expression of glycolysis-related enzymes (LDHA, PFKFB3, PKM2) in BMSCs under normal and HG inflammatory microenvironment. **(F)** Western blot analysis confirmed changes in glycolysis-related enzymes at the protein level. Full-length blots are presented in Supplementary Fig. S4. **(G)** Quantitative analysis of changes in PKM2 tetramer, PKM2 dimer, and the tetramer/dimer ratio in BMSCs exposed to HG inflammatory conditions with or without shikonin treatment, presented in the bar graphs. **(H)** Representative fluorescence images and 3D surface images demonstrate the therapeutic effects of shikonin (Nucleus: blue, PKM2: red; scale bar: 100 μm). * $P < 0.05$, ** $P < 0.01$, *** $P < 0.001$, **** $P < 0.0001$; ns, not significant

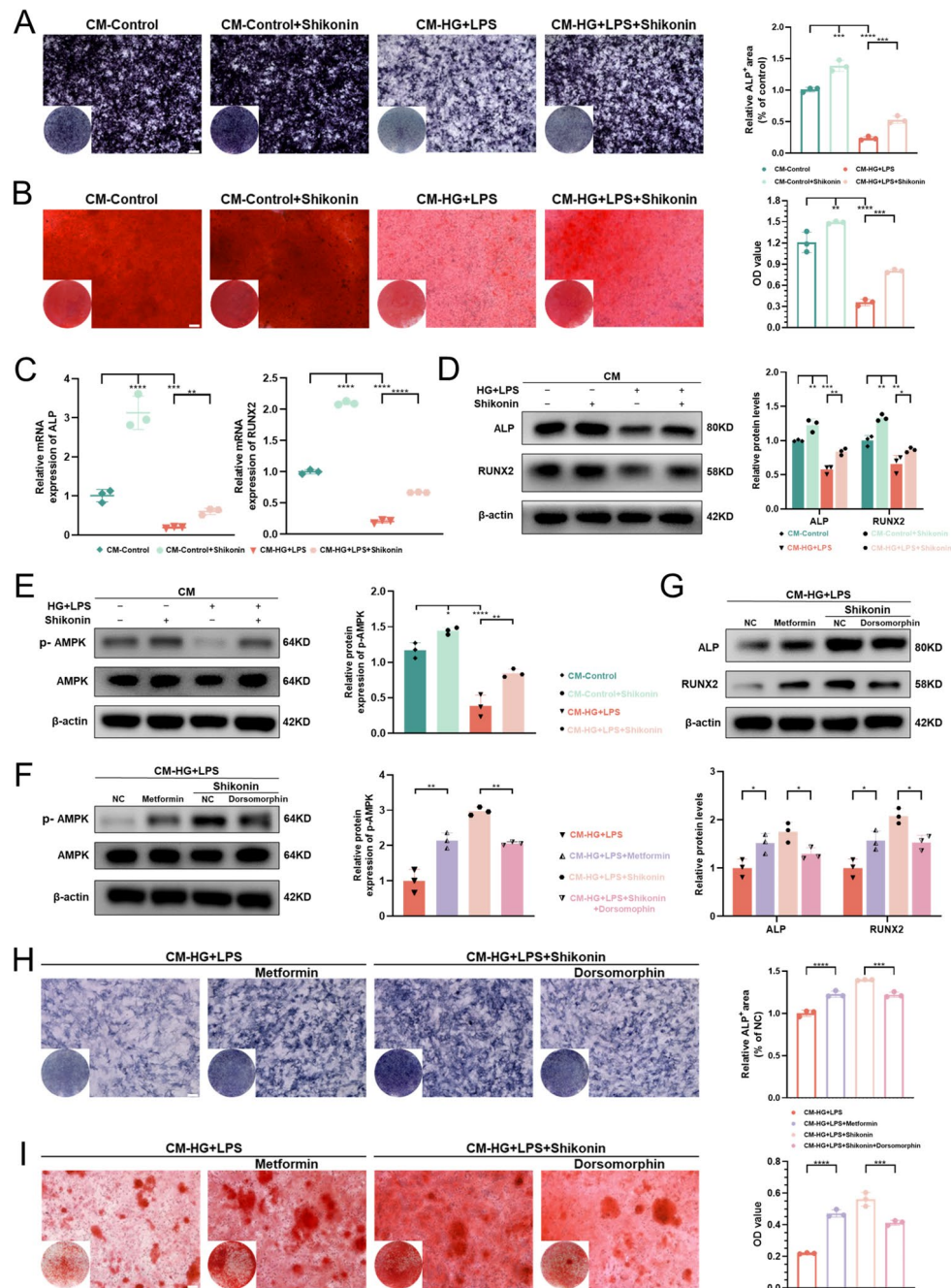


Fig. 7 Shikonin alleviates the inhibition of osteogenic function of BMSCs by activating the AMPK pathway. (**A, B**) ALP and ARS staining results after 7 and 14 days of osteogenic induction using shikonin. Semiquantitative analysis of ALP staining and calcium deposition is shown in the bar charts. (scale bar: 100 μ m). (**C, D**) Effect of shikonin on osteogenesis-related genes and proteins of BMSCs exposed to the HG inflammatory environment or not. Full-length blots are presented in Supplementary Fig. S5. (**E**) Western blot analysis showing AMPK pathway activation following shikonin treatment. Full-length blots are presented in Supplementary Fig. S5. (**F, G**) Western blot bands representing the effects of an AMPK activator and inhibitor (**F**), and the correlation between AMPK activation and osteogenesis (**G**). Full-length blots are presented in Supplementary Fig. S5. (**H, I**) ALP staining and ARS staining images with semi-quantitative analysis. (scale bar: 100 μ m). * $P < 0.05$, ** $P < 0.01$, *** $P < 0.001$, **** $P < 0.0001$; ns, not significant

potential of BMSCs in the HG inflammatory condition (Fig. 7F, G). ALP and ARS staining provided visual confirmation of BMSCs osteogenic function (Fig. 7H, I).

Shikonin reduces alveolar bone loss in diabetic periodontitis mice and promotes periodontal tissue remodeling

We further evaluated the therapeutic effect of shikonin through in vivo experiments. First, we successfully established a T2DM mouse model (Fig. S2A, B) and subsequently induced periodontitis (Fig. S2C). The modeling process of the final DP mice is shown in the figure (Fig. 8A). Additionally, we evaluated the performance of F127DA loaded with shikonin to confirm its feasibility as a drug carrier (Fig. S2D-F).

Micro-CT and histological analyses determined the effect of shikonin on alveolar bone resorption following the induction of DP. As shown in the 3D reconstruction images, the alveolar bone loss in EP and DP mice was severe, but shikonin treatment significantly reduced alveolar bone loss in DP mice. Similar trends were observed in the sagittal view (Fig. 8B). The distance from the CEJ-ABC is an important indicator of periodontal attachment loss, which we used to quantify the extent of periodontal bone resorption. Compared to the control group, both the EP and DP groups had considerably longer distances from CEJ to ABC. Conversely, after shikonin treatment, this distance greatly decreased. Furthermore, microstructural parameters such as bone volume fraction (BV/TV), trabecular number (Tb.N), and trabecular thickness (Tb.Th) are useful indicators of alveolar bone quality. Similarly, shikonin treatment showed higher BV/TV, Tb.N, and Tb.Th (Fig. 8C). HE staining yielded similar results (Fig. 8D). These results indicate that shikonin effectively alleviates alveolar bone loss in DP mice. Masson staining revealed that in the EP and DP groups, periodontal inflammation led to the deformation and degradation of collagen and elastic fibers, ultimately causing sparse and disordered fiber arrangements. Shikonin, on the other hand, resulted in a denser fiber density and better tissue structure in the periodontal ligament of DP mice (Fig. 8E). The presence of diabetes exacerbated the extent of periodontal destruction, leading to increased osteoclast activation; however, shikonin reduced the number of osteoclasts (Fig. 8F). Immunohistochemical staining showed that, compared to the control group, the expression of RUNX2 decreased in the DM, EP, and DP groups, with the most significant effect in the DP group, while shikonin effectively increased the expression of RUNX2. Meanwhile, PKM2 expression exhibited an opposite trend to that of RUNX2 across groups, with shikonin substantially inhibiting PKM2 expression. Interestingly, we also found high expression of PKM2 in areas of inflammation (such as the gums) (Fig. 8G).

Immunofluorescence double staining confirmed a negative correlation between the osteogenic marker OCN and PKM2 in the periodontal area, with shikonin promoting osteogenesis after inhibiting PKM2 (Fig. 8H). In summary, we believe that shikonin may play a key role in the treatment of DP.

Discussion

Diabetes has been clearly established as a major risk factor for periodontitis [29]. Compared to non-diabetic patients, the risk of periodontitis increases approximately threefold in diabetic patients [30]. As a systemic factor, diabetes alters the local microenvironment of periodontitis, potentially diminishing the alveolar bone's self-repair and regeneration capabilities by primarily influencing the osteogenic ability of BMSCs through synergistic inflammatory factors, thereby accelerating the progression of periodontitis. In severe diabetic periodontitis, blood glucose levels above 30 mM and strong LPS-induced inflammatory responses are often observed [31, 32]. Based on clinical relevance and prior studies [33, 34], we selected HG (35 mM) and LPS (1 μ g/mL) as stimuli. However, some in vitro studies have found that stimulation by HG or inflammatory factors promotes osteogenic differentiation [35, 36]. This isolated effect may not represent the multi-factorial environment within. The diabetic periodontal immune microenvironment involves various cellular interactions, with macrophages playing a crucial role in regulating immune responses to periodontal pathogens and bone resorption [37, 38]. Numerous experiments have shown that LPS treatment can increase the secretion of inflammatory factors such as TNF- α and IL-1 β by macrophages [39–41]. Additionally, cytokines secreted by macrophages in response to other external stimuli can induce phenotypic changes in tissue cells [42, 43]. Therefore, culturing BMSCs in the presence of macrophage-conditioned media better simulates the complexity of the periodontal microenvironment in diabetic periodontitis patients. RAW264.7 cells are a well-established murine macrophage cell line, widely used in research related to diabetes and periodontitis due to their strong response to external stimuli and their ability to secrete large amounts of pro-inflammatory cytokines [44, 45]. As a result, we cultured BMSCs using CM from RAW264.7 cells and found that the addition of HG environment exacerbated the destructive effects of the inflammatory conditions. Specifically, CM-HG + LPS treatment severely impaired BMSCs viability and osteogenic function, with PKM2 mediating metabolic reprogramming and mitochondrial dysfunction during osteogenic differentiation. In recent years, increasing evidence has shown that stem cell differentiation is linked to energy metabolism [46, 47]. BMSCs primarily rely on glycolysis for energy to maintain pluripotency when

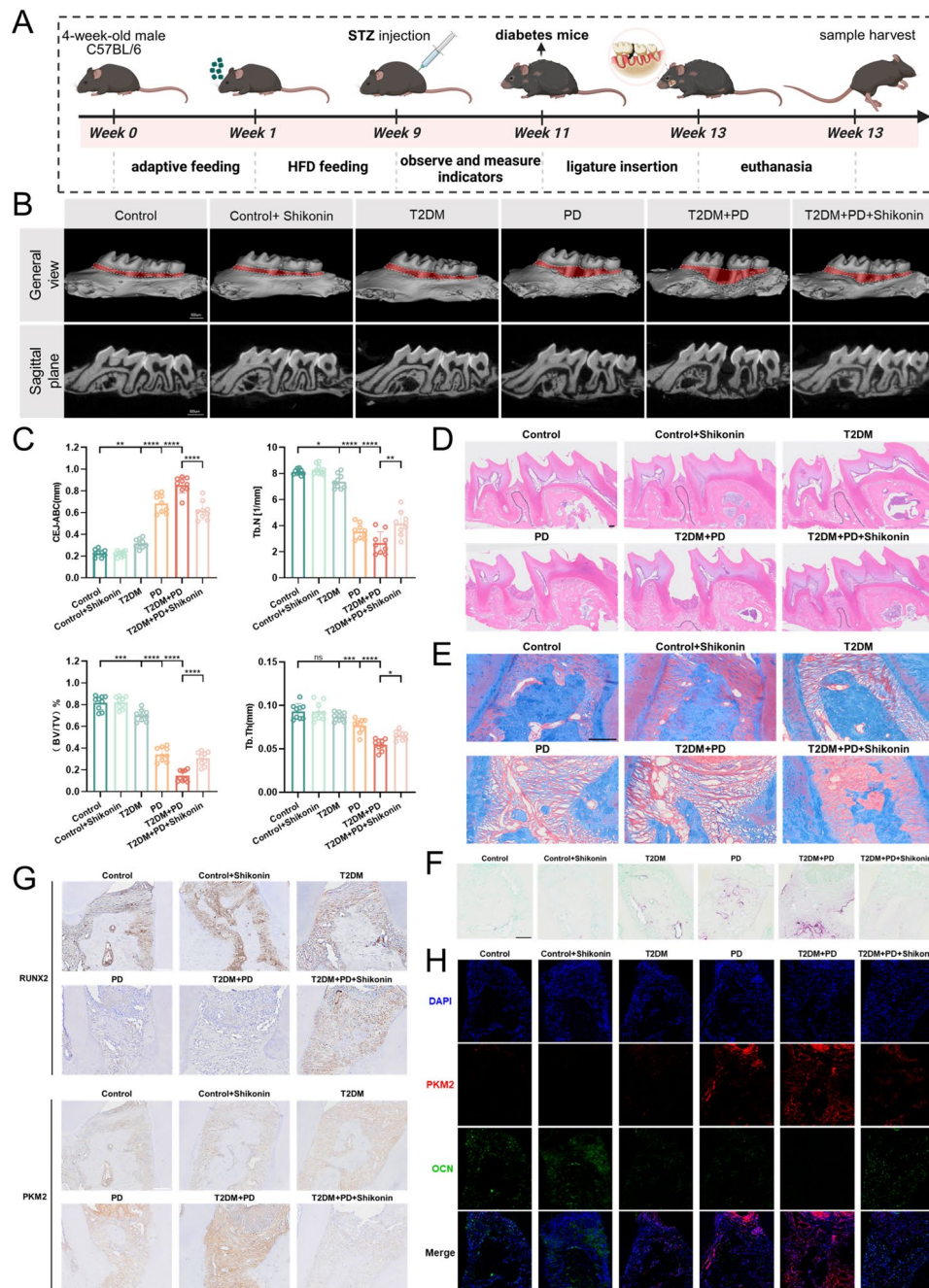


Fig. 8 Shikonin reduces alveolar bone loss in diabetic periodontitis mice and promotes periodontal tissue remodeling. **(A)** Schematic diagram of modeling process of diabetes periodontitis mice (Images created with Biorender.com). **(B)** Micro-CT images of alveolar bone in each group, including 3D and sagittal views. Red areas indicate the extent of exposed tooth roots. **(C)** Analysis of the CEJ-ABC distance and the bone morphological parameters of the alveolar bone in each group. **(D-F)** H&E, Masson, and TRAP staining of periodontal tissue. (scale bar: 100 μ m). **(G)** Representative IHC staining images of RUNX2 and PKM2 in periodontal tissue. (scale bar: 100 μ m). **(H)** IF staining of OCN and PKM2 in the periodontal region. (Nucleus: blue, PKM2: red, OCN: green; scale bar: 100 μ m). * P < 0.05, ** P < 0.01, *** P < 0.001, **** P < 0.0001; ns, not significant

undifferentiated. During the osteogenic differentiation of BMSCs, the OXPHOS process is activated, and BMSCs depend on OXPHOS to meet the high ATP requirements for extracellular matrix protein synthesis [48–50]. The literature confirms that HG can promote cellular glycolysis [51, 52], while inflammatory factor stimulation

can severely block mitochondrial respiration, leading to mitochondrial damage, oxidative stress, and reduced ATP production [53, 54]. Our study demonstrated that CM-HG + LPS treatment induces excessive glycolysis while simultaneously interfering with the OXPHOS pathway, causing cellular stress and forcing increased

reliance on glycolysis, thereby further disrupting metabolic balance via PKM2. (Although no differences in OCR were observed by day 3 of osteogenic induction). A reasonable explanation is that BMSCs initially increase glycolysis to produce ATP more rapidly in response to stress from the HG inflammatory condition [55], maintaining self-renewal or immune regulatory capabilities; this transient stimulation does not affect their OXPHOS pathway. However, long-term exposure to such harsh conditions impairs mitochondrial function in differentiating BMSCs, thus affecting the OXPHOS pathway. To compensate for the decreased ATP due to mitochondrial dysfunction, glycolysis compensatorily increases. This low-efficiency energy production not only requires the cells to take up more glucose but also leads to extracellular lactate accumulation.

PKM2 was found to play a central regulatory role in the metabolic reprogramming of various cell types, through mechanisms such as its expression, activity, allosteric regulation, post-translational modifications, and translocation [56]. Our interest lies in its role in stem cell metabolism. Previous studies have shown that PKM2 can directly bind to gastric cancer-associated transcript 2 (GACAT2), translocating to the mitochondria to enhance OXPHOS in periodontal ligament stem cells (PDLSCs) [57]. A reduction in PKM2 activity can initiate metabolic reprogramming in cancer stem cells, suppressing their malignant biological characteristics [58]. In our study, we observed that inhibiting PKM2 activity and expression could reverse the abnormal upregulation of glycolysis. It is known that PKM2 tetramers have higher enzymatic activity than its dimers and monomers. The highly catalytic tetramer mainly acts in the cytoplasm and has a stronger affinity for the metabolic substrate phosphoenolpyruvate, thereby promoting glycolysis [59, 60]. To assess the allosteric regulatory state of PKM2, we used DSS crosslinking to simultaneously determine the monomeric, dimeric, and tetrameric forms of PKM2 protein in BMSCs. The results showed that the HG inflammatory environment could modulate the conformation of PKM2, considerably increasing the tetramer ratio, indicating activation of the glycolytic pathway. Furthermore, we conducted preliminary exploration of PKM2 localization within cells using immunofluorescence and observed that its intracellular distribution appears to be associated with its conformation. This suggests that PKM2 may undergo translocation by altering its conformation, enabling interactions with other proteins. However, more robust genetic models are needed to confirm this possibility. In future studies, we plan to further investigate the biological effects of PKM2 by isolating subcellular fractions to assess its expression in greater detail.

Successful differentiation of BMSCs relies on proper mitochondrial function, and the balance between

mitochondrial fission and fusion is crucial for maintaining mitochondrial quality and function. Imbalances in mitochondrial dynamics can lead to mitochondrial dysfunction [61]. Undifferentiated BMSCs exhibit an active cell cycle, during which mitochondria are often in a fission state associated with cell division. When BMSCs undergo osteogenic differentiation, they rely on mitochondrial fusion and elongation to maintain mitochondrial function and support OXPHOS, thereby generating more energy required for the differentiation process [62, 63]. This experiment demonstrated that HG inflammatory environment causes mitochondrial dysfunction in BMSCs during osteogenic differentiation, resulting in excessive fragmentation mediated by PKM2. The close relationship between PKM2 and mitochondrial function is increasingly being validated [24]; in this study, we found that inhibiting PKM2 expression can rescue the excessively fragmented mitochondria and upregulate the expression of mitochondrial fusion proteins. Some studies back up this finding [64, 65]. Interestingly, some researchers have proposed the opposite viewpoint, confirming that upregulated PKM2 promotes mitochondrial fusion [19, 66]. We speculate that the explanation for this discrepancy is that different mitochondrial morphologies correspond to the physiological needs of different cells and complicated external surroundings, suggesting that PKM2 does not simply regulate mitochondrial dynamics.

Shikonin is a lipophilic naphthoquinone derived from the herb *Lithospermum erythrorhizon*, and it has been reported to possess various medicinal properties, including anti-inflammatory, anticancer, and antimicrobial effects [67, 68]. Shikonin and its analogs exhibit promising selectivity toward PKM2, as they act on PKM2 without inhibiting the activities of PKM1 and PKL [69]. This experiment confirmed that shikonin regulates mitochondrial function and metabolic characteristics of BMSCs by inhibiting PKM2, thereby promoting osteogenic differentiation through AMPK pathway activation. One study indicated that shikonin may modulate the allosteric structure of PKM2 by forming hydrogen bonds and promoting macromolecular aggregation, while inhibiting its pyruvate kinase activity and protein kinase activity [70]. In vivo animal experiments suggested a unique therapeutic effect of shikonin on diabetic periodontitis mice, as localized application of shikonin significantly improved the damage to mouse periodontal tissue caused by the hyperglycemic inflammatory microenvironment and promoted periodontal bone remodeling.

Currently, the role of PKM2 in diabetic complications is increasingly recognized, revealing promising therapeutic strategies. PKM2 overexpression is linked to diabetic Parkinson's disease (PD) [66], where shikonin inhibits PKM2 to enhance neuronal tolerance to 6-OHDA and lower PD risk in diabetic rats. In diabetic ApoE^{-/-} mice, salvianolic

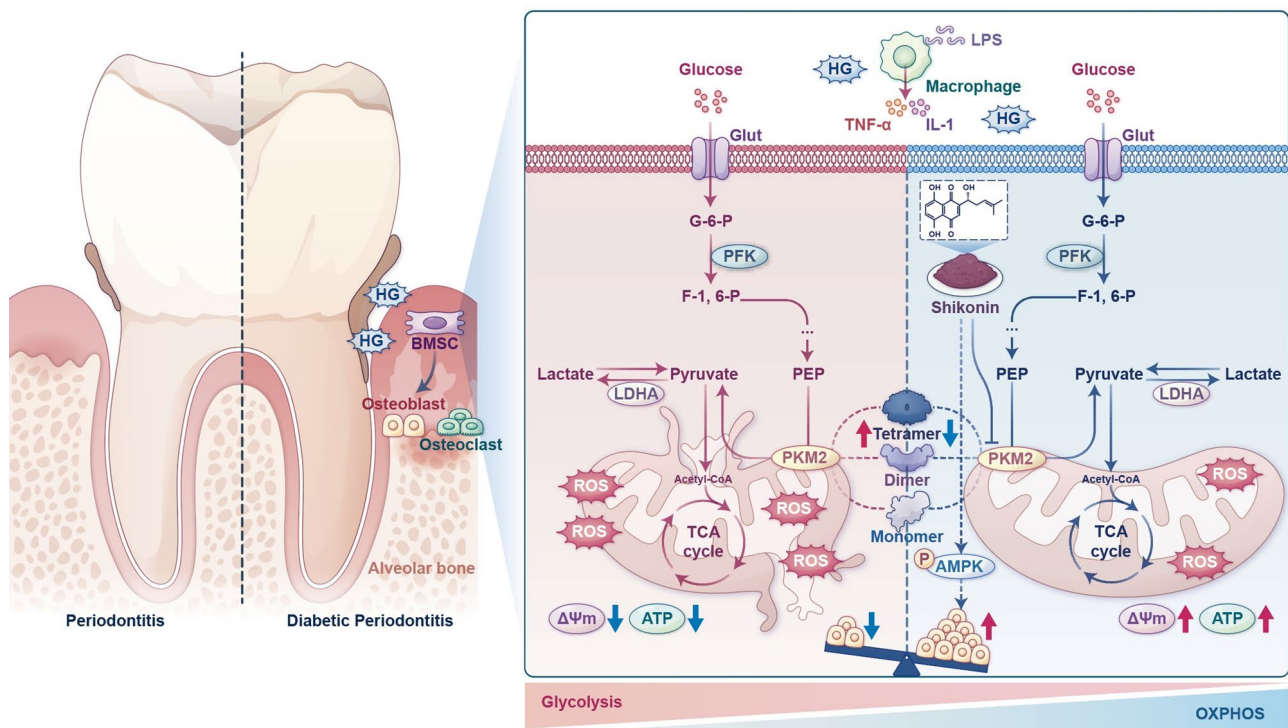


Fig. 9 Graphical Summary

acid A reduces PKM2/PKR-mediated endothelial cell pyroptosis, offering potential for diabetic atherosclerosis treatment [71]. Additionally, the PKM2 activator TEPP-46 prevents diabetic nephropathy by enhancing glucose flux and mitochondrial biogenesis [60]. These findings highlight the importance of PKM2-targeted therapies, although further safety evaluations and animal model studies are needed to validate their potential for clinical application.

In summary, we primarily explored the specific mechanisms by HG inflammatory microenvironment on the osteogenic function of BMSCs from the perspective of metabolic reprogramming, finding that it is related to the upregulated PKM2-mediated hyperglycolysis. Subsequent experiments confirmed that PKM2 has a regulatory effect on mitochondrial function. Treatment with the PKM2 inhibitor shikonin partially restored mitochondrial function and reversed cellular metabolic characteristics, which facilitated periodontal bone regeneration. Nonetheless, the mechanisms underlying the role of osteoclasts in the HG inflammatory environment remain insufficiently explored. Future studies should focus on osteoclast metabolism and the therapeutic effects of shikonin on these cells. Overall, our research provides a potential strategy for the treatment of diabetic periodontitis, but further validation from a more comprehensive perspective is required to confirm its efficacy.

Conclusions

This study explored the destructive effect of HG inflammatory environment on the function of BMSCs and the metabolic and mitochondrial dynamics changes caused by the abnormal up regulation of PKM2. The use of the inhibitor shikonin can effectively save the osteogenic function of BMSCs, which provides a promising method for the treatment of bone regeneration of DP (Fig. 9).

Abbreviations

DM	Diabetes mellitus
PKM2	Pyruvate kinase M2
HG	High-glucose
BMSCs	Bone marrow mesenchymal stem cells
CM	Conditioned media
LPS	Lipopolysaccharide
CCK8	Cell Counting Kit 8
EdU	5-Ethynyl-2'-deoxyuridine
ALP	Alkaline phosphatase
ARS	Alizarin Red S
RUNX2	Runt-related transcription factor 2
ATP	Adenosine triphosphate
2-NBDG	2-Deoxy-2-[(7-nitro-2,1,3-benzoxadiazol-4-yl)amino]-D-glucose
OXPPOS	Oxidative phosphorylation
OCR	Oxygen consumption rate
ECAR	Extracellular acidification rate
FCCP	Trifluoromethoxy carbonyl cyanide phenylhydrazine
2DG	2-Deoxy-d-glucose
LDHA	Lactate dehydrogenase A
PFKFB3	6-phosphofructo-2-kinase/fructose-2,6-biphosphatase 3
MMP	Mitochondrial membrane potential
ROS	Reactive oxygen species
TEM	Transmission electron microscopy
MFN2	Mitofusin-2

OPA1	Optic atrophy 1
DRP1	Dynamin-related protein 1
FIS1	Fission 1
AMPK	AMP-activated protein kinase
DP	Diabetic periodontitis
MCSs	Mesenchymal stem cells
DSS	Disuccinimidyl suberate
T2DM	Mouse model of type 2 diabetes
EP	Experimental periodontitis
F127DA	Polyether F127 diacrylate
OGTT	Oral glucose tolerance test
CEJ-ABC	Distance from the cementoamel junction to the alveolar bone crest
BV/TV	Percentage of bone volume per unit tissue volume
Tb.N	Number of trabeculae
Tb.Th	Trabecular thickness
H&E	Hematoxylin and eosin
EDTA	Ethylene diamine tetraacetie acid
TRAP	Tartrate-resistant acid phosphatase
PDLSCs	Periodontal ligament stem cells
PD	Parkinson's disease
6-OHDA	6-hydroxydopamine

Supplementary Information

The online version contains supplementary material available at <https://doi.org/10.1186/s13287-025-04301-w>.

- Supplementary Material 1
- Supplementary Material 2
- Supplementary Material 3
- Supplementary Material 4
- Supplementary Material 5
- Supplementary Material 6
- Supplementary Material 7
- Supplementary Material 8
- Supplementary Material 9

Acknowledgements

We acknowledge the reviewers for their helpful comments. The authors declare that they have not used AI-generated work in this manuscript.

Author contributions

YZ designed the study and performed most of the experiments. YY provided technical assistance for histomorphology research. YL contributed to the experimental materials support. ZY and XG critically revised manuscript and gave final approval of manuscript. JZ guided the research and provided final approval of manuscript.

Funding

This work was supported by the National Natural Science Foundation of China (No. 81901038), the Natural Science Foundation of Chongqing (No. cstc2019jcyj-msxmX0174) and the Chongqing Medical Scientific Research Project(No. 2024MSXM075).

Data availability

The datasets used and/or analyzed during the current study are available from the corresponding author on reasonable request. All additional files are included in the manuscript.

Declarations

Ethics approval and consent to participate

All animal procedures have been approved by the Animal Ethics Committee of Chongqing Medical University (Project: The Role of PKM2-Mediated Metabolic Reprogramming in the Osteogenic Differentiation of BMSCs under Diabetic Periodontitis Conditions, No. 2024-115, Date: 2024.07.19), and are in compliance with the Guidelines for ethical review of animal welfare of Laboratory animals issued by the China National Standardization Management Committee (publication No. GB/T35892-2018). This research did not use any human cells/tissues/samples/cell lines.

Consent for publication

Not applicable.

Competing interests

The authors declare that they have no competing interests.

Author details

¹College of Stomatology, Chongqing Medical University, 426# Songshibei Road, Yubei District, Chongqing 401147, P.R. China

²Chongqing Key Laboratory of Oral Diseases and Biomedical Sciences, Chongqing, China

³Chongqing Municipal Key Laboratory of Oral Biomedical Engineering of Higher Edcation, Chongqing, China

Received: 13 November 2024 / Accepted: 1 April 2025

Published online: 18 April 2025

References

1. Loe H. Periodontal disease. The sixth complication of diabetes mellitus. *Diabetes Care*. 1993;16(1):329–34.
2. Graves DT, Ding Z, Yang Y. The impact of diabetes on periodontal diseases. *Periodontol* 2000. 2020;82(1):214–24. <https://doi.org/10.1111/prd.12318>.
3. Lalla E, Papapanou PN. Diabetes mellitus and periodontitis: a Tale of two common interrelated diseases. *Nat Rev Endocrinol*. 2011;7(12):738–48. <https://doi.org/10.1038/nrendo.2011.106>.
4. Confavreux CB, Levine RL, Karsenty G. A paradigm of integrative physiology, the crosstalk between bone and energy metabolisms. *Mol Cell Endocrinol*. 2009;310(1–2):21–9. <https://doi.org/10.1016/j.mce.2009.04.004>.
5. Liu K, Cao J, Shi X, Wang L, Zhao T. Cellular metabolism and homeostasis in pluripotency regulation. *Protein Cell*. 2020;11(9):630–40. <https://doi.org/10.1007/s13238-020-00755-1>.
6. Meacham CE, DeVilbiss AW, Morrison SJ. Metabolic regulation of somatic stem cells in vivo. *Nat Rev Mol Cell Biol*. 2022;23(6):428–43. <https://doi.org/10.1038/s41580-022-00462-1>.
7. Li X, Jiang O, Wang S. Molecular mechanisms of cellular metabolic homeostasis in stem cells. *Int J Oral Sci*. 2023;15(1):52. <https://doi.org/10.1038/s41368-023-00262-z>.
8. Stegen S, Carmeliet G. Metabolic regulation of skeletal cell fate and function. *Nat Rev Endocrinol*. 2024;20(7):399–413. <https://doi.org/10.1038/s41574-024-00969-x>.
9. Yoshida GJ. Metabolic reprogramming: the emerging concept and associated therapeutic strategies. *J Exp Clin Cancer Res* CR. 2015;34:111. <https://doi.org/10.1186/s13046-015-0221-y>.
10. Wculek SK, Heras-Murillo I, Mastrangelo A, Mañanes D, Galán M, Miguel V, et al. Oxidative phosphorylation selectively orchestrates tissue macrophage homeostasis. *Immunity*. 2023;56(3):516–e5309. <https://doi.org/10.1016/j.immuni.2023.01.011>.
11. Zhang Z, Deng X, Liu Y, Liu Y, Sun L, Chen F. PKM2, function and expression and regulation. *Cell Biosci*. 2019;9:52. <https://doi.org/10.1186/s13578-019-0317-8>.
12. Hu K, Yang Y, Lin L, Ai Q, Dai J, Fan K, et al. Caloric restriction mimetic 2-Deoxyglucose alleviated inflammatory lung injury via suppressing nuclear pyruvate kinase M2-Signal transducer and activator of transcription 3 pathway. *Front Immunol*. 2018;9:426. <https://doi.org/10.3389/fimmu.2018.00426>.
13. Alquraishi M, Chahed S, Alani D, Puckett DL, Dowker PD, Hubbard K, et al. Podocyte specific deletion of PKM2 ameliorates LPS-induced podocyte injury through beta-catenin. *Cell Commun Signal CCS*. 2022;20(1):76. <https://doi.org/10.1186/s12964-022-00884-6>.

14. Palsson-McDermott EM, Curtis AM, Goel G, Lauterbach MAR, Sheedy FJ, Gleeson LE, et al. Pyruvate kinase M2 regulates Hif-1 α activity and IL-1 β induction and is a critical determinant of the Warburg effect in LPS-activated macrophages. *Cell Metab*. 2015;21(1):65–80. <https://doi.org/10.1016/j.cmet.2014.12.005>.
15. Zong Y, Li H, Liao P, Chen L, Pan Y, Zheng Y, et al. Mitochondrial dysfunction: mechanisms and advances in therapy. *Signal Transduct Target Ther*. 2024;9(1):124. <https://doi.org/10.1038/s41392-024-01839-8>.
16. Chouchani ET, Pell VR, James AM, Work LM, Saeb-Parsy K, Frezza C, et al. A unifying mechanism for mitochondrial superoxide production during Ischemia-Reperfusion injury. *Cell Metab*. 2016;23(2):254–63. <https://doi.org/10.1016/j.cmet.2015.12.009>.
17. Sorrentino V, Romani M, Mouchiroud L, Beck JS, Zhang H, D'Amico D, et al. Enhancing mitochondrial proteostasis reduces amyloid- β proteotoxicity. *Nature*. 2017;552(7684):187–93. <https://doi.org/10.1038/nature25143>.
18. Li T, Han J, Jia L, Hu X, Chen L, Wang Y. PKM2 coordinates Glycolysis with mitochondrial fusion and oxidative phosphorylation. *Protein Cell*. 2019;10(8):583–94. <https://doi.org/10.1007/s13238-019-0618-z>.
19. Ren R, Guo J, Shi J, Tian Y, Li M, Kang H. PKM2 regulates angiogenesis of VREPCs through modulating glycolysis, mitochondrial fission, and fusion. *J Cell Physiol*. 2020;235(9):6204–17. <https://doi.org/10.1002/jcp.29549>.
20. Li M, Xing X, Huang H, Liang C, Gao X, Tang Q, et al. BMS-2 Derived apoE promotes craniofacial bone repair via ROS/JNK signaling. *J Dent Res*. 2022;101(6):714–23. <https://doi.org/10.1177/00220345211068338>.
21. Marchesan J, Ginary MS, Jing L, Miao MZ, Zhang S, Sun L, et al. An experimental murine model to study periodontitis. *Nat Protoc*. 2018;13(10):2247–67. <https://doi.org/10.1038/s41596-018-0035-4>.
22. Zeng Y, Pan Q, Wang X, Li D, Lin Y, Man F, et al. Impaired mitochondrial fusion and oxidative phosphorylation triggered by high glucose is mediated by Tom22 in endothelial cells. *Oxid Med Cell Longev*. 2019;2019:4508762. <https://doi.org/10.1155/2019/4508762>.
23. Jitschin R, Böttcher M, Saul D, Lukassen S, Bruns H, Loschinski R, et al. Inflammation-induced glycolytic switch controls suppressivity of mesenchymal stem cells via STAT1 glycosylation. *Leukemia*. 2019;33(7):1783–96. <https://doi.org/10.1038/s41375-018-0376-6>.
24. Gao J, Zhao Y, Li T, Gan X, Yu H. The role of PKM2 in the regulation of mitochondrial function: focus on mitochondrial metabolism, oxidative stress, dynamic, and apoptosis. PKM2 in mitochondrial function. *Oxid Med Cell Longev*. 2022;2022:7702681. <https://doi.org/10.1155/2022/7702681>.
25. Herzig S, Shaw RJ. AMPK: guardian of metabolism and mitochondrial homeostasis. *Nat Rev Mol Cell Biol*. 2018;19(2):121–35. <https://doi.org/10.1038/nrm.2017.95>.
26. Huang J, Liu K, Zhu S, Xie M, Kang R, Cao L, et al. AMPK regulates immunometabolism in sepsis. *Brain Behav Immun*. 2018;72:89–100. <https://doi.org/10.1016/j.bbi.2017.11.003>.
27. Jayabalan J, Shah M, Viollet B, Chenu C. AMP-activated protein kinase pathway and bone metabolism. *J Endocrinol*. 2012;212(3):277–90. <https://doi.org/10.1530/JOE-11-0306>.
28. Chen L, Shi X, Xie J, Weng SJ, Xie ZJ, Tang JH, et al. Apelin-13 induces mitophagy in bone marrow mesenchymal stem cells to suppress intracellular oxidative stress and ameliorate osteoporosis by activation of AMPK signaling pathway. *Free Radic Biol Med*. 2021;163:356–68. <https://doi.org/10.1016/j.free-radbiomed.2020.12.235>.
29. Salvi GE, Carollo-Bittel B, Lang NP. Effects of diabetes mellitus on periodontal and peri-implant conditions: update on associations and risks. *J Clin Periodontol*. 2008;35(8 Suppl):398–409. <https://doi.org/10.1111/j.1600-051X.2008.01282.x>.
30. Mealey BL, Ocampo GL. Diabetes mellitus and periodontal disease. *Periodontol*. 2007;44:127–53. <https://doi.org/10.1111/j.1600-0757.2006.00193.x>.
31. Simpson TC, Clarkson JE, Worthington HV, MacDonald L, Weldon JC, Needleman I, et al. Treatment of periodontitis for glycaemic control in people with diabetes mellitus. *Cochrane Database Syst Rev*. 2022;4(4):CD004714. <https://doi.org/10.1002/14651858.CD004714.pub4>.
32. Salvi GE, Collins JG, Yalda B, Arnold RR, Lang NP, Offenbacher S. Monocytic TNF alpha secretion patterns in IDDM patients with periodontal diseases. *J Clin Periodontol*. 1997;24(1):8–16. <https://doi.org/10.1111/j.1600-051x.1997.tb01178.x>.
33. Yang S, Yin Y, Sun Y, Ai D, Xia X, Xu X, et al. AZGP1 aggravates macrophage M1 polarization and pyroptosis in periodontitis. *J Dent Res*. 2024;103(6):631–41. <https://doi.org/10.1177/00220345241235616>.
34. Zhou M, Xu X, Li J, Zhou J, He Y, Chen Z, et al. C-reactive protein perturbs alveolar bone homeostasis: an experimental study of periodontitis and diabetes in the rat. *J Clin Periodontol*. 2022;49(10):1052–66. <https://doi.org/10.1111/jcpe.13667>.
35. Seubbuk S, Sritanaudomchai H, Kasetsuwan J, Surarit R. High glucose promotes the osteogenic differentiation capability of human periodontal ligament fibroblasts. *Mol Med Rep*. 2017;15(5):2788–94. <https://doi.org/10.3892/mmr.2017.6333>.
36. He W, Wang Z, Luo Z, Yu Q, Jiang Y, Zhang Y, et al. LPS promote the odontoblastic differentiation of human dental pulp stem cells via MAPK signaling pathway. *J Cell Physiol*. 2015;230(3):554–61. <https://doi.org/10.1002/jcp.24732>.
37. Mo K, Wang Y, Lu C, Li Z. Insight into the role of macrophages in periodontitis restoration and development. *Virulence*. 2024;15(1):2427234. <https://doi.org/10.1080/21505594.2024.2427234>.
38. Zhuang Z, Yoshizawa-Smith S, Glowacki A, Maltos K, Pacheco C, Shehabeldin M, et al. Induction of M2 macrophages prevents bone loss in murine periodontitis models. *J Dent Res*. 2019;98(2):200–8. <https://doi.org/10.1177/0022034518805984>.
39. Torretta S, Scagliola A, Ricci L, Mainini F, Di Marco S, Cuccovillo I, et al. D-mannose suppresses macrophage IL-1 β production. *Nat Commun*. 2020;11(1):6343. <https://doi.org/10.1038/s41467-020-20164-6>.
40. Chu K, Zhang Z, Chu Y, Xu Y, Yang W, Guo L. Ginsenoside Rg1 alleviates lipopolysaccharide-induced pyroptosis in human periodontal ligament cells via inhibiting Drp1-mediated mitochondrial fission. *Arch Oral Biol*. 2023;147:105632. <https://doi.org/10.1016/j.archoralbio.2023.105632>.
41. Lu MK, Lee MH, Chao CH, Hsu YC. Sodium sulfate addition increases the bioresource of biologically active sulfated polysaccharides from antrodia cinnamomea. *Int J Biol Macromol*. 2024;257(Pt 2):128699. <https://doi.org/10.1016/j.jbiomac.2023.128699>.
42. Zhao P, Yue Z, Nie L, Zhao Z, Wang Q, Chen J, et al. Hyperglycaemia-associated macrophage pyroptosis accelerates periodontal inflamm-aging. *J Clin Periodontol*. 2021;48(10):1379–92. <https://doi.org/10.1111/jcpe.13517>.
43. Li Z, Bratlie KM. Fibroblasts treated with macrophage conditioned medium results in phenotypic shifts and changes in collagen organization. *Mater Sci Eng C Mater Biol Appl*. 2021;122:111915. <https://doi.org/10.1016/j.msec.2021.111915>.
44. Liu H, Liu Y, Fan W, Fan B. Fusobacterium nucleatum triggers Proinflammatory cell death via Z-DNA binding protein 1 in apical periodontitis. *Cell Commun Signal CCS*. 2022;20(1):196. <https://doi.org/10.1186/s12964-022-01005-z>.
45. Sun X, Ma Z, Zhao X, Jin W, Zhang C, Ma J, et al. Three-dimensional Bioprinting of multicell-laden scaffolds containing bone morphogenic protein-4 for promoting M2 macrophage polarization and accelerating bone defect repair in diabetes mellitus. *Bioact Mater*. 2021;6(3):757–69. <https://doi.org/10.1016/j.bioactmat.2020.08.030>.
46. Ning K, Liu S, Yang B, Wang R, Man G, Wang DE, et al. Update on the effects of energy metabolism in bone marrow mesenchymal stem cells differentiation. *Mol Metab*. 2022;58:101450. <https://doi.org/10.1016/j.molmet.2022.101450>.
47. van Gestel N, Carmeliet G. Metabolic regulation of skeletal cell fate and function in physiology and disease. *Nat Metab*. 2021;3(1):11–20. <https://doi.org/10.1038/s42255-020-00321-3>.
48. Chen CT, Shih YRV, Kuo TK, Lee OK, Wei YH. Coordinated changes of mitochondrial biogenesis and antioxidant enzymes during osteogenic differentiation of human mesenchymal stem cells. *Stem Cells Dayt Ohio*. 2008;26(4):960–8. <https://doi.org/10.1634/stemcells.2007-0509>.
49. Shum LC, White NS, Mills BN, Bentley KL, de Eliseev M. Energy metabolism in mesenchymal stem cells during osteogenic differentiation. *Stem Cells Dev*. 2016;25(2):114–22. <https://doi.org/10.1089/scd.2015.0193>.
50. Tencerova M, Rendina-Ruedy E, Neess D, Faergeman N, Figeac F, Ali D, et al. Metabolic programming determines the lineage-differentiation fate of murine bone marrow stromal progenitor cells. *Bone Res*. 2019;7:35. <https://doi.org/10.1038/s41413-019-0076-5>.
51. Han CY, Umemoto T, Omer M, Den Hartigh LJ, Chiba T, LeBoeuf R, et al. NADPH oxidase-derived reactive oxygen species increases expression of monocyte chemotactic factor genes in cultured adipocytes. *J Biol Chem*. 2012;287(13):10379–93. <https://doi.org/10.1074/jbc.M111.304998>.
52. Guntur AR, Gerencser AA, Le PT, DeMambro VE, Bornstein SA, Mookerjee SA, et al. Osteoblast-like MC3T3-E1 cells prefer Glycolysis for ATP production but Adipocyte-like 3T3-L1 cells prefer oxidative phosphorylation. *J Bone Min Res Off J Am Soc Bone Min Res*. 2018;33(6):1052–65. <https://doi.org/10.1002/jbmr.3390>.
53. Zhao W, Xu Z, Cao J, Fu Q, Wu Y, Zhang X, et al. Elamipretide (SS-31) improves mitochondrial dysfunction, synaptic and memory impairment induced by

- lipopolysaccharide in mice. *J Neuroinflammation*. 2019;16(1):230. <https://doi.org/10.1186/s12974-019-1627-9>.
54. Choumar A, Tarhuni A, Lett ron P, Reyl-Desmars F, Dauhoo N, Damasse J, et al. Lipopolysaccharide-induced mitochondrial DNA depletion. *Antioxid Redox Signal*. 2011;15(11):2837–54. <https://doi.org/10.1089/ars.2010.3713>.
55. Yang J, Ueharu H, Mishina Y. Energy metabolism: A newly emerging target of BMP signaling in bone homeostasis. *Bone*. 2020;138:115467. <https://doi.org/10.1016/j.bone.2020.115467>.
56. Patel S, Das A, Meshram P, Sharma A, Chowdhury A, Jariyal H, et al. Pyruvate kinase M2 in chronic inflammations: a potpourri of crucial protein-protein interactions. *Cell Biol Toxicol*. 2021;37(5):653–78. <https://doi.org/10.1007/s10565-021-09605-0>.
57. Li X, Tian BM, Deng DK, Liu F, Zhou H, Kong DQ, et al. LncRNA GACAT2 binds with protein PKM1/2 to regulate cell mitochondrial function and cementogenesis in an inflammatory environment. *Bone Res*. 2022;10(1):29. <https://doi.org/10.1038/s41413-022-00197-x>.
58. Zhao H, Jiang R, Feng Z, Wang X, Zhang C. Transcription factor LHX9 (LIM homeobox 9) enhances pyruvate kinase PKM2 activity to induce glycolytic metabolic reprogramming in cancer stem cells, promoting gastric cancer progression. *J Transl Med*. 2023;21(1):833. <https://doi.org/10.1186/s12967-023-04658-7>.
59. Wu B, Liang Z, Lan H, Teng X, Wang C. The role of PKM2 in cancer progression and its structural and biological basis. *J Physiol Biochem*. 2024;80(2):261–75. <https://doi.org/10.1007/s13105-024-01007-0>.
60. Qi W, Keenan HA, Li Q, Ishikado A, Kannt A, Sadowski T, et al. Pyruvate kinase M2 activation May protect against the progression of diabetic glomerular pathology and mitochondrial dysfunction. *Nat Med*. 2017;23(6):753–62. <https://doi.org/10.1038/nm.4328>.
61. Li Q, Gao Z, Chen Y, Guan MX. The role of mitochondria in osteogenic, adipogenic and chondrogenic differentiation of mesenchymal stem cells. *Protein Cell*. 2017;8(6):439–45. <https://doi.org/10.1007/s13238-017-0385-7>.
62. Forni MF, Peggion J, Trudeau K, Shirihai O, Kowaltowski AJ. Murine mesenchymal stem cell commitment to differentiation is regulated by mitochondrial dynamics. *Stem Cells Dayt Ohio*. 2016;34(3):743–55. <https://doi.org/10.1002/stem.2248>.
63. Wang Y, Barthez M, Chen D. Mitochondrial regulation in stem cells. *Trends Cell Biol*. 2024;34(8):685–94. <https://doi.org/10.1016/j.tcb.2023.10.003>.
64. Ding Z, Da HH, Osama A, Xi J, Hou Y, Fang J. Emodin ameliorates antioxidant capacity and exerts neuroprotective effect via PKM2-mediated Nrf2 transactivation. *Food Chem Toxicol Int J Publ Br Ind Biol Res Assoc*. 2022;160:112790. <https://doi.org/10.1016/j.fct.2021.112790>.
65. Xie W, He Q, Zhang Y, Xu X, Wen P, Cao H, et al. Pyruvate kinase M2 regulates mitochondrial homeostasis in cisplatin-induced acute kidney injury. *Cell Death Dis*. 2023;14(10):663. <https://doi.org/10.1038/s41419-023-06195-z>.
66. Zhao Y, Wang Y, Wu Y, Tao C, Xu R, Chen Y, et al. PKM2-mediated neuronal hyperglycolysis enhances the risk of Parkinson's disease in diabetic rats. *J Pharm Anal*. 2023;13(2):187–200. <https://doi.org/10.1016/j.jpha.2022.11.006>.
67. Guo C, He J, Song X, Tan L, Wang M, Jiang P, et al. Pharmacological properties and derivatives of shikonin-A review in recent years. *Pharmacol Res*. 2019;149:104463. <https://doi.org/10.1016/j.phrs.2019.104463>.
68. Sun Q, Gong T, Liu M, Ren S, Yang H, Zeng S, et al. Shikonin, a naphthalene ingredient: therapeutic actions, pharmacokinetics, toxicology, clinical trials and pharmaceutical researches. *Phytomedicine*. 2022;94:153805. <https://doi.org/10.1016/j.phymed.2021.153805>.
69. Chen J, Xie J, Jiang Z, Wang B, Wang Y, Hu X. Shikonin and its analogs inhibit cancer cell Glycolysis by targeting tumor pyruvate kinase-M2. *Oncogene*. 2011;30(42):4297–306. <https://doi.org/10.1038/onc.2011.137>.
70. Huang B, Wang Q, Jiang L, Lu S, Li C, Xu C, et al. Shikonin ameliorated mice colitis by inhibiting dimerization and tetramerization of PKM2 in macrophages. *Front Pharmacol*. 2022;13:926945. <https://doi.org/10.3389/fphar.2022.926945>.
71. Zhu J, Chen H, Le Y, Guo J, Liu Z, Dou X, et al. Salvianolic acid A regulates pyroptosis of endothelial cells via directly targeting PKM2 and ameliorates diabetic atherosclerosis. *Front Pharmacol*. 2022;13:1009229. <https://doi.org/10.3389/fphar.2022.1009229>.

Publisher's note

Springer Nature remains neutral with regard to jurisdictional claims in published maps and institutional affiliations.